Dr. Lundquist

1075

5/46

NATIONAL ADVISORY COMMITTEE FOR AERONAUTICS

TECHNICAL NOTE

No. 1075

EFFECT OF COMPRESSIBILITY ON SECTION CHARACTERISTICS OF AN AIRFOIL WITH A ROUND-NOSE SLOTTED FRISE AILERON

By Arvo A. Luoma

Langley Memorial Aeronautical Laboratory
Langley Field, Va.

Washington
May 1946

NATIONAL ADVISORY COMMITTEE FOR AERONAUTICS

TECHNICAL NOTE No. 1075

EFFECT OF COMPRESSIBILITY ON SECTION CHARACTERISTICS OF AN AIRFOIL WITH A ROUND-NOSE SLOTTED FRISE AILERON

By Arvo A. Luoma

SUMMARY

Compressibility effects on the aerodynamic section characteristics of an airfoil with a round-nose slotted Frise aileron were investigated from pressure distributions obtained at various airfoil angles of attack and aileron angles for Mach numbers from 0.25 to approximately 0.76. The aileron tested represented a modification of a sharp-nose Frise aileron previously investigated by the NACA. The modification included an increased nose radius as well as an increased balance chord.

Modifying the nose of the aileron improved the section aileron effectiveness $\Delta\alpha/\Delta\delta_a$ at large negative aileron deflections and slightly reduced the effectiveness at moderate aileron deflections. The wind-tunnel data indicated a reduction in stick force and an improvement in stick-force characteristics at high diving speeds; however, the tendency of the up-going aileron toward excessive overbalance at these high speeds still existed. Section aileron loads were essentially unchanged by modifying the aileron nose.

INTRODUCTION

Flight tests of a high-speed, fighter-type airplane with sharp-nose ailerons showed heavy stick forces at large aileron deflections and undesirable aileron overbalance tendencies in high-speed dives. These aileron difficulties were further evidenced by the results of the high-speed tunnel tests (reference 1) of an aileron model based on the midsection of the original sharp-nose aileron used on this airplane. In order to improve the lateral-control characteristics of the airplane, the

Langley Flight Research Division modified the original aileron by increasing the nose radius and nose overhang. Flight tests of this modified aileron were made and reported in reference 2.

The high-speed-tunnel tests of the sharp-nose aileron model reported in reference 1 were extended to include tests of an aileron model based on the midsection of the NACA modified aileron developed for use on a high-speed fighter-type airplane. Complete pressure-distribution measurements over the main portion of the airfoil and modified aileron were made at Mach numbers up to approximately 0.76 to determine the aerodynamic section characteristics of the airfoil and aileron and the effect of compressibility upon these characteristics.

SYMBOLS

The term "airfoil" is herein used to mean the combination of the aileron and the main portion of the airfoil. The term "aileron alone" refers to the characteristics of the aileron in the presence of the main portion of the airfoil. The aerodynamic coefficients and other symbols used in the present report are as follows:

α	angle of attack
V	velocity in undisturbed stream
p'	rolling angular velocity
p	local static pressure at a point on airfoil section
p_o	static pressure in undisturbed stream
ρ	mass density in undisturbed stream
a	speed of sound in undisturbed stream
q	dynamic pressure in undisturbed stream $\left(\frac{1}{2}\rho V^2\right)$
P	pressure coefficient $\left(\frac{p - p_o}{q}\right)$
M	Mach number (V/a)

δ_a aileron deflection; positive for down deflection

c_a total chord of aileron (see fig. 1)

c_M chord of main portion of airfoil (without aileron)

c_w chord of airfoil (with aileron)

x distance along chord from leading edge of airfoil or aileron

x_{h_a} hinge-axis location along chord from leading edge of aileron

x_{h_w} hinge-axis location along chord from leading edge of airfoil

y distance normal to chord

y_h hinge-axis location normal to chord

c_{n_a} section normal-force coefficient of aileron alone from pressure-distribution data

$$c_{n_a} = \frac{1}{c_a} \int_0^{c_a} \left(P_L - P_U\right) dx$$

c_{n_M} section normal-force coefficient of main portion of airfoil (without aileron) from pressure-distribution data

$$c_{n_M} = \frac{1}{c_M} \int_0^{c_M} \left(P_L - P_U\right) dx$$

c_{n_w} section normal-force coefficient of airfoil (with aileron) from pressure-distribution data; component of total normal-force coefficient due to aileron chord force neglected; maximum absolute error thus introduced approximately 0.01

$$c_{n_w} = \frac{1}{c_w} \left(c_M c_{n_M} + c_a c_{n_a} \cos \delta_a\right)$$

c_{c_a} section chord-force coefficient of aileron alone from pressure-distribution data

$$c_{c_a} = \frac{1}{c_a}\int_{y_{min}}^{y_{max}} \left(P_{ah} - P_r\right) dy$$

c_{h_a} section hinge-moment coefficient of aileron alone about aileron hinge axis from pressure-distribution data

$$c_{h_a} = \left(\frac{1}{c_a}\right)^2\left[\int_0^{c_a} \left(P_U - P_L\right)\left(x - x_{h_a}\right) dx + \int_{y_{min}}^{y_{max}} \left(P_{ah} - P_r\right)\left(y - y_h\right) dy\right]$$

c_m section pitching-moment coefficient of airfoil (with aileron) about quarter-chord point of airfoil due to normal force on main portion of airfoil and aileron; pitching moment due to chord force of main portion of airfoil and aileron not included

$$c_m = \left(\frac{1}{c_w}\right)^2\left[\int_0^{c_M} \left(P_U - P_L\right)\left(x - \frac{c_w}{4}\right) dx + \int_0^{c_a}\left(P_U - P_L\right)\left(x - x_{h_a}\right) dx - c_{n_a}c_a \cos \delta_a \left(x_{h_w} - \frac{c_w}{4}\right) + c_{n_a}c_a \sin \delta_a\, y_h\right]$$

c_{p_a} section center-of-pressure coefficient of aileron alone (ratio of distance of center of pressure of aileron from leading edge of aileron to total chord of aileron)

Subscripts:

cr when local speed of sound has been reached on some point on airfoil section

U upper surface of airfoil section

L lower surface of airfoil section

ah ahead of maximum ordinates of aileron

r to the rear of maximum ordinates of aileron

max maximum

min minimum

APPARATUS AND TESTS

The tests were made in the Langley 8-foot high-speed tunnel, which is of the single-return, circular cross-section, closed-throat type with continuously controlled airspeed for these tests in an approximate Mach number range of 0.15 to 0.75.

The model used in this investigation was a 24-inch-chord 10.5-percent-thick airfoil with a round-nose slotted Frise aileron based on the midsection of the NACA modified aileron developed for a high-speed fighter-type airplane. The model was of uniform section and spanned the tunnel. The main portion of the airfoil and the aileron tailpiece were the same as those used in the tests of reference 1. The sharp nosepiece of the aileron of reference 1 was replaced with a nosepiece of increased nose radius and increased nose overhang. The aileron hinge-axis location, with respect to airfoil chord, remained the same for both models. A cross section of the modified round-nose aileron discussed herein is compared with the original aileron in figure 1. Tables I and II give the coordinates of the main portion of the airfoil and the modified aileron, respectively. The aileron nose radius was increased from 0.4 of 1 percent of the aileron chord for the original sharp-nose aileron to 2.2 percent of the aileron chord for the modified aileron.

The additional nose overhang increased the original aileron chord by 2 percent and changed the geometric nose balance from 25.70 percent to 27.16 percent.

Complete static-pressure measurements over the main portion of the airfoil and the aileron were made for Mach numbers from 0.25 to approximately 0.76 for various airfoil angles of attack and aileron deflections. The tests were made with aileron deflections from -15.5° to 15°. Model structural considerations limited the maximum aileron deflections to values less than those of reference 1. Simultaneous observations of the static pressures acting over the airfoil were obtained by photographing a multiple-tube liquid manometer.

RESULTS

The aerodynamic section characteristics presented herein have been determined from integration of pressure-distribution data by the same method used in the analysis of the data of reference 1.

Section airfoil normal-force coefficient c_{n_w} is plotted against angle of attack α at various aileron deflections in figure 2. Compressibility effects on section normal-force-curve slope $\partial c_{n_w}/\partial \alpha$ and $\partial c_{n_w}/\partial \delta_a$ are shown in figure 3.

The effectiveness of the aileron for producing roll is indicated by figure 4, which shows the variation in angle of attack with aileron deflection necessary to maintain a section airfoil normal-force coefficient of 0. A large negative slope is necessary for high rate of roll. The effect of compressibility on aileron effectiveness for moderate aileron deflections is more fully brought out in figure 5, which shows the variation of the effectiveness ratio $\Delta\alpha/\Delta\delta_a$ (here taken as the average value for deflections from -6° to 6°; the minus sign is omitted) with Mach number. Figure 6 is a plot of section steady rate of roll against Mach number. This section roll varies directly as the product of the effectiveness ratio $\Delta\alpha/\Delta\delta_a$ and the velocity V and was determined as

explained in reference 1. The section roll is proportional to the roll of a rigid wing in pure roll; therefore, figure 6 has been included to illustrate the nature of the compressibility effect on roll.

Section aileron hinge-moment-coefficient data are given in figures 7 and 8 and section center-of-pressure coefficient data in figure 9. Estimated stick-force data for nondifferential aileron deflections, based on hinge-moment coefficients at airfoil lift coefficients corresponding to those of a high-speed fighter-type airplane in level flight, are given in figure 10. These data were calculated for an aileron linkage of 1.7° aileron deflection per inch of stick movement, an area of the single aileron of 13.3 square feet, an aileron mean chord of 19.1 inches, and a hinge-axis location 27.2 percent back from the leading edge of the aileron. No account has been taken of variation of the section aileron geometric balance along the aileron span or of the effect of three-dimensional flow on actual stick forces.

Comparative data on peak negative pressure coefficients (here taken as peak experimental values at a static orifice) for the subject aileron and that reported in reference 1 are shown in figure 11. The data for the modified aileron at aileron deflections of -12° and -15.5° are shown extrapolated, where necessary, to the P_{cr}-curve. Figure 12 gives section aileron critical Mach number data. Section aileron normal-force coefficient data and section aileron loading data are presented in figures 13 and 14, respectively.

Figure 15 shows data on section critical Mach number of the main portion of the airfoil. Section airfoil pitching-moment-coefficient data appear in figure 16 and section aileron chord-force coefficient data in figure 17.

Included in some of these figures are curves taken from reference 1 for the original sharp-nose aileron. These data are presented for comparative purposes, and the sharp-nose aileron is designated the original aileron (reference 1).

DISCUSSION

The nosepiece of the aileron used in these tests had a larger nose radius and more nose overhang than that used in the tests of reference 1, as previously mentioned and shown in figure 1. This change in nose form, of course, modified the shape of the slot between the main portion of the airfoil and the aileron nose. Except for the different nose shape with its modifying effect on slot shape, the two airfoil models were the same. The discussion is, therefore, chiefly concerned with the effect of modification of the aileron nose radius and geometric balance upon aerodynamic section characteristics of the airfoil and aileron. The results reported for the modified aileron are compared with those presented in reference 1 for the airfoil with the original sharp-nose aileron.

Control Effectiveness Characteristics

The normal-force-curve slopes $\partial c_{n_w}/\partial \alpha$ and $\partial c_{n_w}/\partial \delta_a$ for the modified aileron (figs. 2 and 3) are essentially the same as those given in reference 1 for the original aileron. Improved air flow at large negative aileron deflections renders the modified aileron more effective in producing roll at these deflections than the original aileron, as shown by the larger changes in angle of attack α at large negative deflections necessary to maintain a constant value of section airfoil normal-force coefficient (fig. 4). Hence, at moderate speeds at which stick forces permit aileron deflections of this magnitude, greater rates of roll are indicated for the modified aileron. This difference in effectiveness, however, becomes less with increase in Mach number. For figure 5 the effectiveness ratio $\Delta\alpha/\Delta\delta_a$ at moderate aileron deflections ($\pm 6^\circ$) is found to be somewhat lower for the modified aileron model than for the original aileron model. This loss in effectiveness can be seen to amount to less than 5 percent at a Mach number of 0.7 (figs. 5 and 6). The flight tests of reference 2 showed increased effectiveness at large aileron deflections for the NACA modified ailerons, as indicated by the two-dimensional data, but the flight tests generally showed some improvement at moderate deflections also.

Aileron Hinge-Moment Coefficient

Modification of the aileron has a favorable effect, because of improved flow conditions, on the hinge-moment coefficient of the aileron over an extended range of negative aileron deflections (figs. 7 and 8). The negative aileron deflection, beyond which there is a rapid increase in hinge-moment coefficient, has been increased from -6° deflection for the original aileron to -12° deflection at the lower Mach numbers for the modified aileron (fig. 8), and this extension is desirable in keeping stick forces light over a greater range of aileron deflections. The pressure plots indicate no separation at the lowest Mach number for a deflection of -12°, but some separation off the lower surface occurs at the higher Mach numbers. This tendency toward separation is further evidenced by the increase in hinge-moment coefficient with Mach number (fig. 8) and by the rearward shift in aileron center-of-pressure coefficient with Mach number (fig. 9(a)). For an aileron deflection of -12° the hinge-moment coefficient of the modified aileron at low Mach numbers is appreciably less, even to the point of overbalance, than that of the original aileron. Compressibility effects, however, diminish this difference so that, at a Mach number of 0.6, the hinge-moment coefficient of the modified aileron approaches that of the original aileron. At aileron deflections greater than -12° there is a rapid increase in hinge-moment coefficient (fig. 8) and a rearward shift in center-of-pressure coefficient (fig. 9) due to increased flow separation off the lower surface of the aileron. This separation is aggravated by compressibility. Flight tests of the modified NACA aileron (reference 2) showed improved flow conditions over an even greater range of negative aileron deflections than did the two-dimensional tests. The aileron stick-force data from the flight tests indicate no severe separation off the aileron for aileron deflections up to -15° (maximum deflection tested) at a Mach number of 0.33 (maximum test speed with maximum deflection).

The tendency toward excessive overbalance at high Mach numbers noted in reference 1 for aileron deflections of -4° and -6° is also noted for the modified aileron. Rounding the nose of the aileron delays and makes more gradual the unporting of the aileron nose at up deflections, and this feature lessens the undesirable tendencies

of an aileron of this type to "snatch". A high-speed fighter airplane equipped with a set of NACA modified ailerons has been dived, with ailerons kept approximately neutral, to a Mach number of 0.86 without showing aileron snatch or any of the other objectionable features characteristic of the original sharp-nose ailerons in high-speed dives. The tendency toward excessive overbalance at high Mach numbers, however, is still to be expected with any type of control surface that depends upon a nose form which protrudes into the air stream for close aerodynamic balance. For positive aileron deflections the hinge-moment coefficient (fig. 8) and the center-of-pressure coefficient (fig. 9) of the modified aileron show characteristics similar to those of the original aileron; the hinge moments for the modified aileron, however, are somewhat less.

Undesirable stick-force characteristics at the highest Mach numbers, where in a region of moderate aileron deflections the stick force decreased with increasing deflection as a result of the tendency of the up-going aileron toward excessive overbalance, were noted in reference 1 for the original aileron. These characteristics were improved in the modified aileron (fig. 10) but extrapolation of the stick-force curves indicates that, at speeds beyond those of the test data, similar control difficulties may be encountered. Estimated stick forces at moderate aileron deflections ($\pm 4^\circ$) were somewhat increased for the modified aileron at the lowest Mach numbers and reduced at the higher Mach numbers. This reduction at the higher Mach numbers, for example, amounts to 13 percent for an aileron deflection of $\pm 4^\circ$ at a Mach number of 0.525. (See fig. 10.) The decrease in stick force at the higher Mach numbers permits greater aileron deflections for the modified aileron at speeds where stick force is the limiting factor determining maximum possible aileron deflection. Although the effectiveness ratio $\Delta\alpha/\Delta\delta_a$ for small deflections is slightly less for the modified aileron, the rate of roll at these speeds can be expected to be increased as a consequence of the larger range of aileron deflections possible.

The hinge-moment-coefficient data of the two-dimensional tests indicated a reduction of stick forces at large aileron deflections as a result of modifying the aileron nose, and this reduction was also shown in the flight tests of reference 2. At moderate aileron deflections there is variance, however, in the effect of

nose modification on estimated stick forces based on two-dimensional data and actual stick forces obtained in flight. Mention has been made previously of reasons for the discrepancy between flight values and those based on two-dimensional data. In addition, with an aileron of the Frise type, small differences in aileron contour, balance, and rigging resulting from manufacturing and assembly irregularities can cause appreciable changes in stick-force values. Stick-force data obtained for an aileron of this type, therefore, apply rigorously only for the particular wing-aileron combination used in the tests and may be quite different for another wing-aileron combination built to the same nominal dimensions. The flight stick-force data of reference 2 are measured from the trim position of the ailerons, and changes in trim position can have notable effect on stick-force magnitudes for a nonlinear variation of hinge-moment coefficient with aileron deflection. The two-dimensional data indicate, for example, that at a Mach number of 0.60 and for a total aileron deflection of 8° from trim position a change in trim from 0° to ± 1° can reduce the stick force by 15 percent.

Frise Aileron Critical Speeds

Increasing the nose radius of the Frise aileron had a marked effect on the magnitudes and variation with Mach number of the peak negative pressures about the aileron nose at large negative aileron deflections. The round nose of the modified aileron retarded flow separation off the lower surface to larger negative deflections with the consequent development of high peak negative pressures about the nose at large deflections, as shown in figure 11. The rapid decrease in peak negative pressures for the -12° aileron deflection, due to compressibility effects, and for the -15.5° deflection, due to both section airfoil normal-force-coefficient variation and compressibility, with the resultant increased tendency toward flow separation is further evidenced by large changes in aileron aerodynamic characteristics, especially hinge-moment coefficients. At negative deflections up to -6° the nose modification produced no large changes in peak negative pressures. Any marked departure of the air flow about a body from the streamline picture, in which the flow follows the contour of the body, results in adverse effects on aerodynamic characteristics. This flow change may

result, at subcritical Mach numbers, from ordinary separation or, at supercritical Mach numbers, from energy losses (that cause incomplete pressure recovery behind the shock) and from separation of the flow as a result of the severe pressure gradients across the shock waves. The critical Mach number of a body refers, of course, to the minimum free-stream Mach number at which the local velocity of the air stream at any point on the body has reached the local speed of sound. For flow that has not separated, the critical Mach number is the criterion for determining the speed at which detrimental flow changes due to compression shock can be expected to develop. The field of supersonic flow over the Frise aileron at up deflections is localized about the nose of the aileron; thus the compression shock losses are not so severe as those on an airfoil where supersonic flow occurs over a much greater extent of surface; but at speeds in excess of the aileron critical speed adverse effects including vibration and shake of the control can well develop. If separation has occurred at subcritical speeds so that the flow is already undesirable, the critical Mach number is no longer of primary interest. In this case, the critical Mach number merely means that a flow, which already is undesirable at subcritical speeds, can be expected to be even worse at supercritical speeds.

Since the critical Mach number corresponds to a unique value of pressure coefficient, variations in critical peak negative pressure coefficient as a result of aileron nose modification will be reflected by corresponding variations in critical Mach number (fig. 12). Because of higher peak pressures about the nose, the critical Mach number of the modified aileron at large up deflections is seen to be lower than that of the original aileron. As has been brought out previously, the air flow about the model with the original aileron at large up deflections is already undesirable at subcritical speeds as a result of severe separation off the aileron. This separation meant reduced negative pressure peaks about the aileron nose and a higher critical speed which in this case, however, is no longer of primary importance since the flow is already undesirable. Nose modification improved flow by delaying separation at large up deflections but with the development of high negative pressures about the aileron nose. For moderate negative aileron deflections (up to -6°), nose modification changed the critical Mach number by a maximum of only 0.025.

For positive aileron deflections two negative pressure peaks occur on the upper surface of the aileron, one at the leading edge and the other 28 to 33 percent behind the leading edge where there is a relatively rapid change in curvature of the upper surface. For the original aileron the maximum negative pressure coefficient occurred at the second of these pressure peaks. The maximum negative pressure coefficient of the modified aileron occured at the first of these peaks, as the increase in nose radius and balance caused an increase in the negative pressure peak at the leading edge. Lower critical Mach numbers for the modified aileron ensued and were also more affected by the section airfoil normal-force coefficient (fig. 12). The maximum decrease in critical Mach number at positive deflections amounted to 0.075 at a deflection of 6°.

If lift effectiveness is to be maintained, separation must not occur. Modifying the aileron nose delayed separation to larger up deflections and consequently improved effectiveness but also increased the peak negative pressure coefficients about the aileron nose. Prevention of separation with a control of the Frise type can therefore be attained only at the expense of the development of high negative pressures about the aileron nose. Instability of the high negative pressures, moreover, produces corresponding undesirable variations in aerodynamic balance and, hence, in hinge-moment characteristics.

Section Aileron Loads

The magnitude of the section aileron normal-force coefficient (fig. 13) was essentially unchanged by the modification of the nose of the aileron except at the largest negative deflections where the loading increased. At the lowest Mach numbers there was also some increase in section aileron normal-force coefficient at positive deflections above 6°, but compressibility effects diminished this difference in the coefficients noted at these Mach numbers. The section aileron loads (fig. 14) were generally somewhat less for the modified aileron for deflections of 4°, 2°, and -12° and somewhat more for deflections of 12°, 6°, 0°, -2°, -4°, and -6°. Modifying the aileron nose increased the loading at up deflections on the forward portion of the aileron but generally decreased the loading on the rear portion. For a

deflection of -12° the decrease in loading on the rear 75 percent of the aileron was sufficient to cause a net decrease in loading as shown in figure 14.

Other Airfoil Characteristics

The modified nose on the aileron produced only small changes in the critical Mach number of the main portion of the airfoil (fig. 15). The largest change was an increase in critical Mach number of 0.02 for the airfoil with the modified aileron at an airfoil normal-force coefficient of 0 and an aileron deflection of -12°. The section pitching-moment-coefficient characteristics (fig. 16) for the modified aileron model are quite similar to those for the original aileron model. There is some difference, at the largest negative aileron deflections where delayed separation on the modified aileron resulted in an increase in pitching-moment coefficient; however, this difference in pitching-moment coefficient is lessened with increase in Mach number since separation off the modified aileron is aggravated by compressibility. The modified nose has appreciable effect on the section aileron chord-force coefficients (fig. 17), and compressibility also has a large additional effect on these chord forces.

CONCLUDING REMARKS

Section airfoil and aileron characteristics were determined from wind-tunnel measurements of the complete pressure distributions over an airfoil with a round-nose slotted Frise aileron (based on the midsection of the NACA modified aileron developed for a high-speed fighter-type airplane) for Mach numbers from 0.25 to approximately 0.76 for various airfoil angles of attack and aileron deflections. The ailerons tested represented a modification of a sharp-nose Frise aileron previously investigated by the NACA. The modification included an increased nose radius as well as an increased balance chord. These tests indicated the following comparative conclusions:

1. The airfoil with the modified aileron can be expected to be more effective for producing roll at large negative aileron deflections than the airfoil with the

original aileron. This difference in effectiveness, however, would become less with increase in Mach number. At moderate aileron deflections ($\pm 6^{\circ}$) a small loss in section aileron effectiveness $\Delta\alpha/\Delta\delta_a$ resulted from modifying the aileron nose.

2. The estimated stick forces for nondifferential aileron deflections were reduced for the modified aileron and, because of the greater range of aileron deflections possible at high speeds at which stick forces become excessive, an improvement in rate of roll is indicated at these speeds.

3. At high diving speeds a tendency of the up-going aileron toward excessive overbalance still exists but modification of the aileron nose improved the stick-force characteristics at these speeds.

4. Section aileron loads were essentially unchanged by modifying the aileron nose.

Langley Memorial Aeronautical Laboratory
National Advisory Committee for Aeronautics
Langley Field, Va., March 7, 1946

REFERENCES

1. Luoma, Arvo A.: Effect of compressibility on Presure Distribution over an Airfoil with a Slotted Frise Aileron. NACA ACR No. L4G12, 1944.

2. Williams, W. C.: A Flight Investigation of NACA Aileron Modifications for the Improvement of the Lateral Control Characteristics of a High-Speed Fighter Airplane. NACA ACR No. L5J29, 1945.

TABLE I

ORDINATES FOR MAIN PORTION OF AIRFOIL (WITHOUT AILERON)

[Stations and ordinates in inches from airfoil L.E. and chord line, respectively]

Station	Ordinate		Station	Ordinate	
	Upper surface	Lower surface		Upper surface	Lower surface
0	-----	-----			
.03	0.11	-0.08	9.50	1.51	-0.91
.15	.27	-.17	10.10	1.47	-.90
.30	.42	-.23	10.69	1.43	-.88
.45	.56	-.28	11.88	1.34	-.83
.59	.67	-.32	13.07	1.23	-.78
.89	.86	-.38	14.26	1.10	-.70
1.19	1.00	-.43	15.45	.98	-.61
1.49	1.12	-.47	16.25	.88	-.55
1.78	1.22	-.51	16.63	.83	-.52
2.08	1.30	-.55	16.78	.82	-.49
2.38	1.37	-.59	16.93	.80	-.43
2.67	1.43	-.62	17.08	.78	-.20
2.97	1.47	-.66	17.23	.77	.04
3.27	1.51	-.69	17.38	.75	.20
3.56	1.54	-.71	17.52	.72	.31
4.16	1.59	-.77	17.67	.71	.39
4.75	1.62	-.82	17.82	.70	.44
5.35	1.63	-.85	17.97	.68	.48
5.94	1.64	-.89	18.12	.66	.50
6.53	1.63	-.90	18.27	.64	.53
7.13	1.62	-.91	18.42	.63	.55
7.72	1.60	-.92	18.56	.61	.56
8.32	1.57	-.91	18.71	.59	.56
8.91	1.54	-.91	18.76	.58	.58

L.E. radius: 0.18 in.
Slope of radius through end of chord: 0.100
Shroud trailing-edge radius: 0.01 in.

NATIONAL ADVISORY
COMMITTEE FOR AERONAUTICS

TABLE II

ORDINATES FOR AILERON ALONE

[Ordinates in inches from chord line]

Nosepiece				Tailpiece			
Station		Ordinate		Station		Ordinate	
(In. from airfoil L.E.)	(In. from aileron L.E.)	Upper surface	Lower surface	(In. from airfoil L.E.)	(In. from aileron L.E.)	Upper surface	Lower surface
17.41	0	-0.30	-0.30	19.75	2.34	0.48	-0.29
17.44	.03	-.19	-.38	19.90	2.49	.47	-.28
17.47	.06	-.15	-.40	20.05	2.64	.45	-.26
17.50	.09	-.12	-.42	20.20	2.79	.42	-.25
17.52	.11	-.10	-.44	20.50	3.09	.39	-.23
17.55	.14	-.07	-.45	20.79	3.38	.35	-.21
17.58	.17	-.05	-.45	21.09	3.68	.31	-.20
17.61	.20	-.04	-.45	21.39	3.98	.27	-.17
17.64	.23	-.02	-.45	21.68	4.27	.23	-.15
17.67	.26	-.01	-.45	21.98	4.57	.20	-.14
17.70	.29	.01	-.45	22.28	4.87	.17	-.12
17.73	.32	.02	-.45	22.57	5.16	.13	-.10
17.76	.35	.03	-.45	22.87	5.46	.10	-.08
17.79	.38	.04	-.44	23.17	5.76	.07	-.06
17.82	.41	.05	-.44	23.47	6.06	.05	-.04
17.97	.56	.10	-.43	23.76	6.35	.02	-.02
18.12	.71	.15	-.42	24.00	6.59	0	0
18.27	.86	.20	-.40				
18.42	1.01	.26	-.39				
18.56	1.15	.30	-.37				
18.71	1.30	.35	-.36				
18.86	1.45	.40	-.35				
19.01	1.60	.45	-.34				
19.16	1.75	.48	-.33				
19.31	1.90	.49	-.32				
19.46	2.05	.50	-.31				
19.60	2.19	.50	-.30				
19.70	2.29	.49	-.29				

NATIONAL ADVISORY
COMMITTEE FOR AERONAUTICS

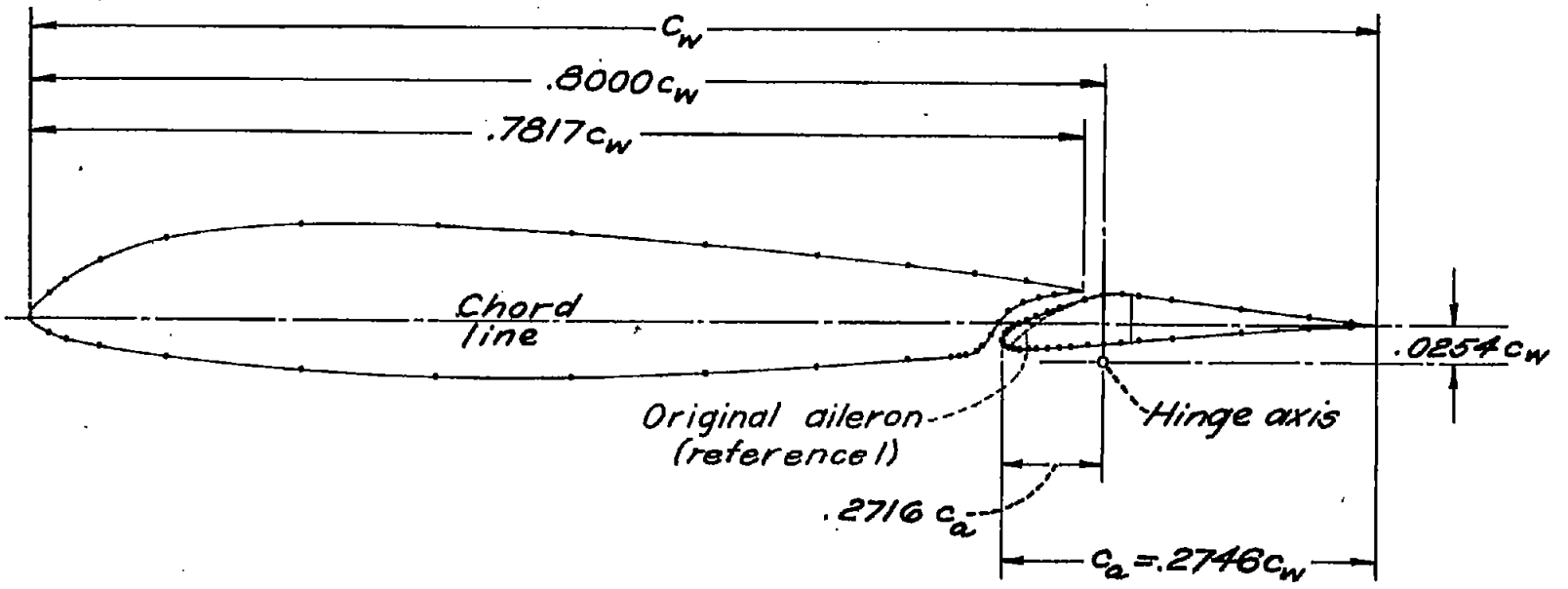

Figure 1.- Cross-section of model based on section of wing of a high-speed fighter-type airplane taken through midsection of NACA modified slotted Frise aileron. Orifice locations indicated.

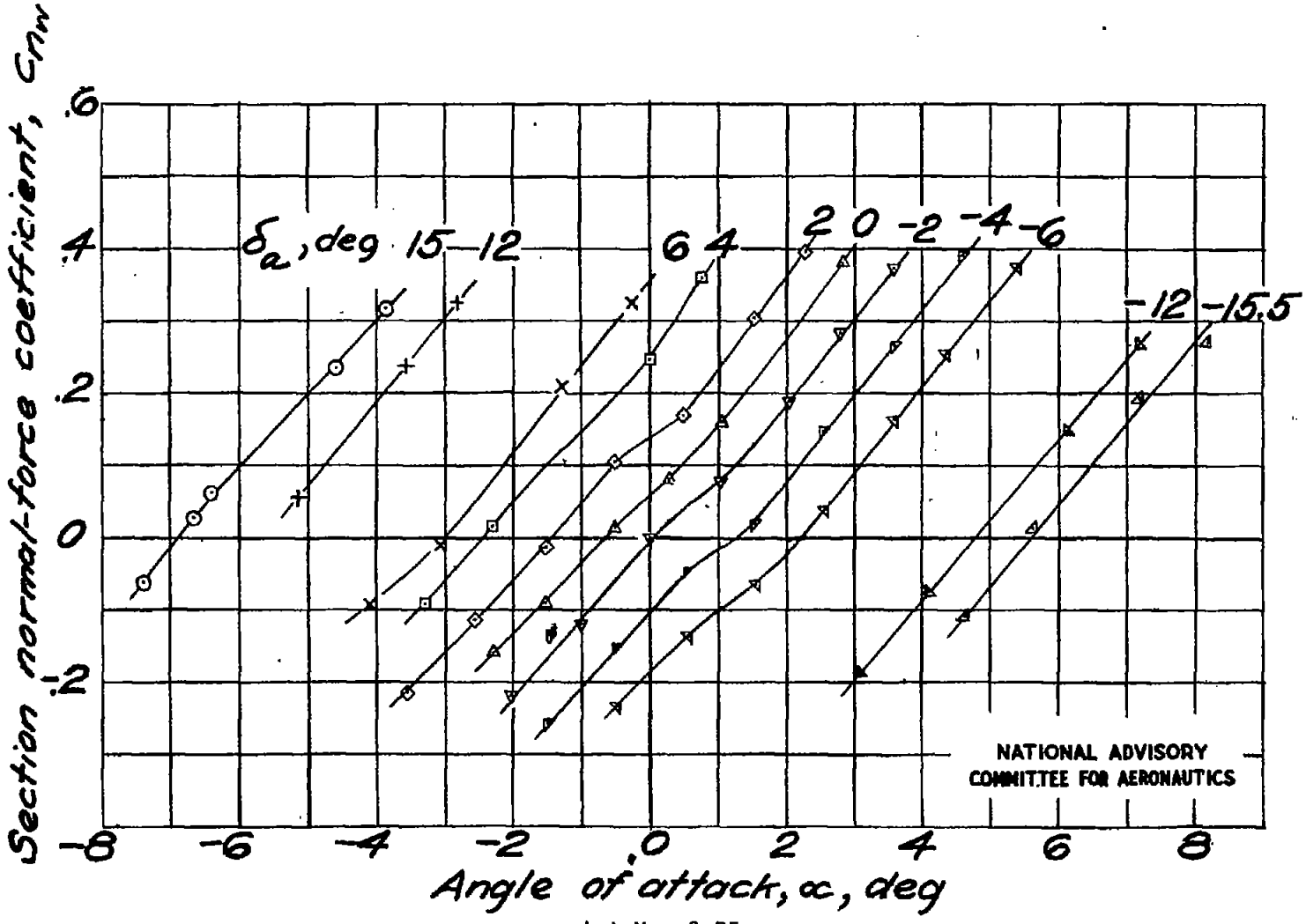

(a) M = 0.25.

Figure 2.- Section airfoil normal-force coefficient against angle of attack at various aileron deflections.

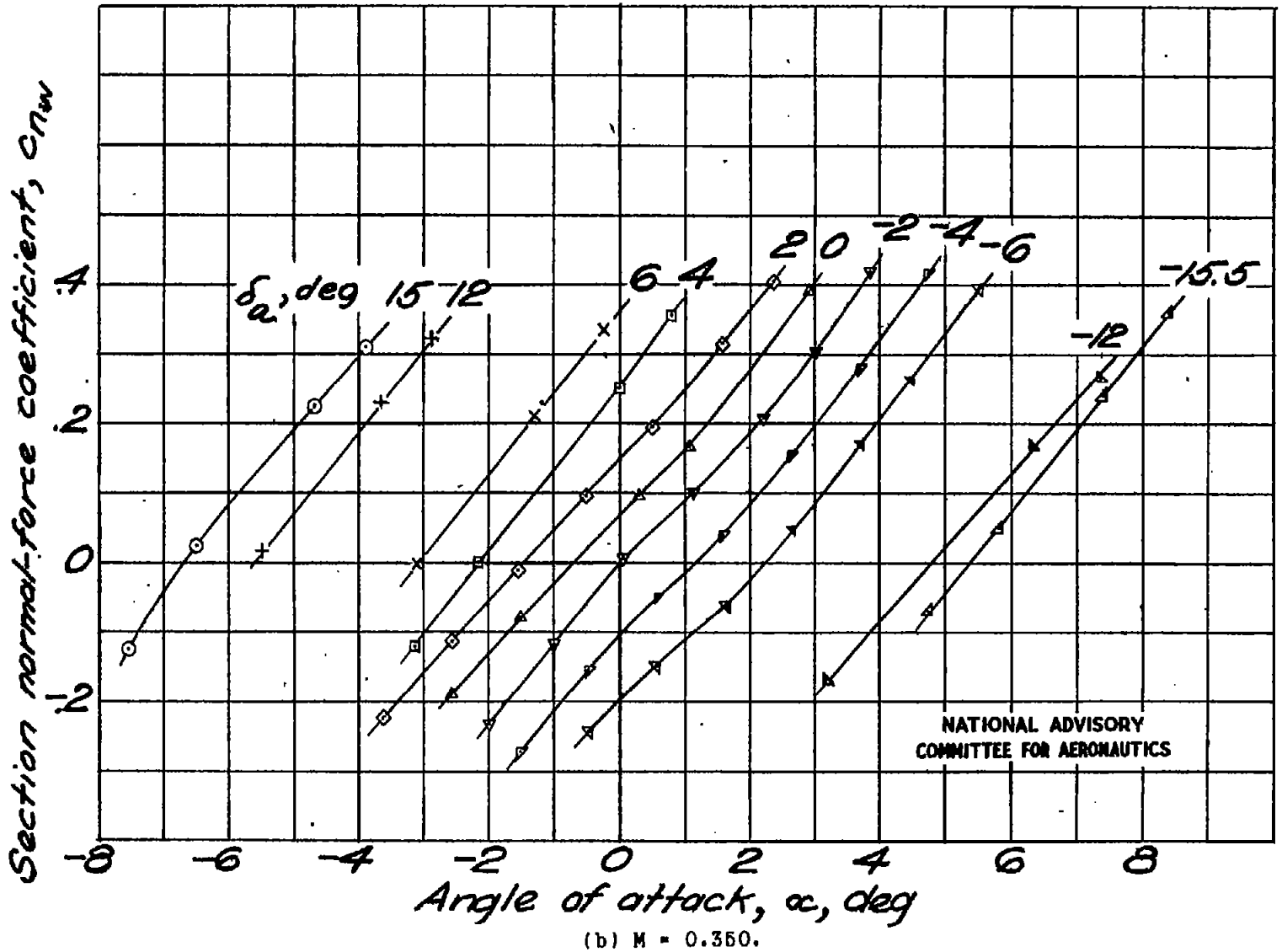

(b) M = 0.350.

Figure 2.- Continued.

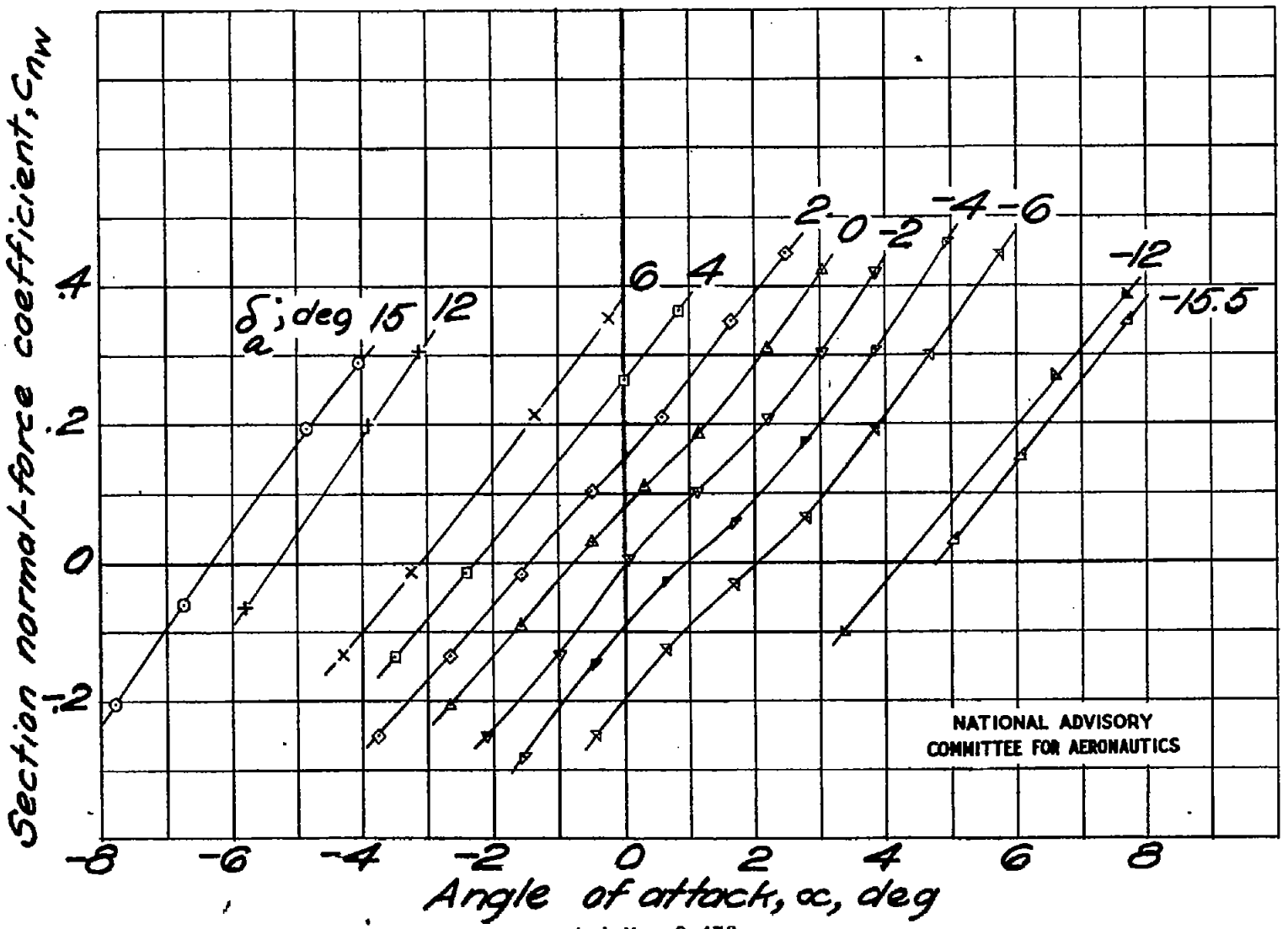

(c) M = 0.470.

Figure 2.- Continued.

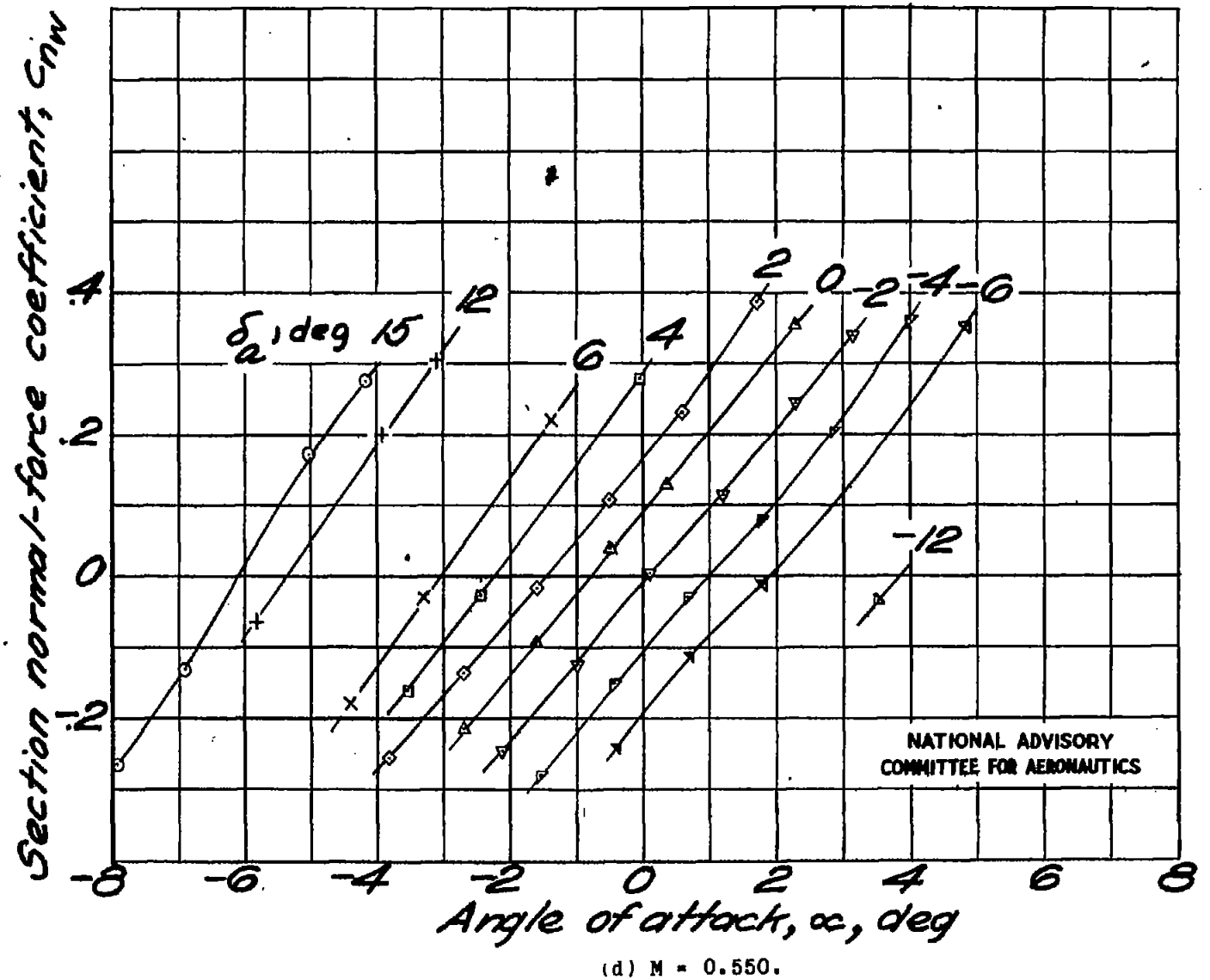

(d) M = 0.550.

Figure 2.- Continued.

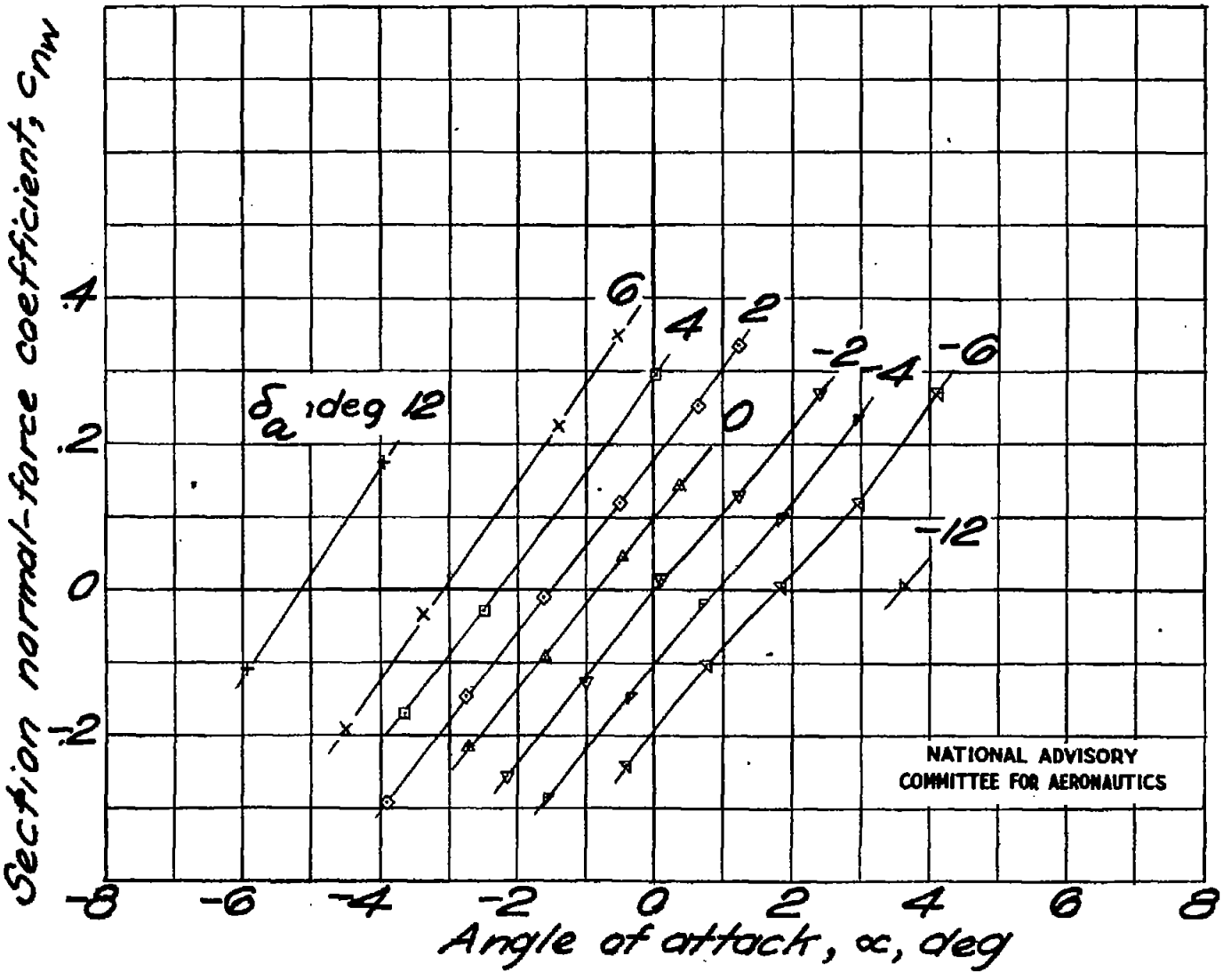

(e) M = 0.600.

Figure 2.- Continued.

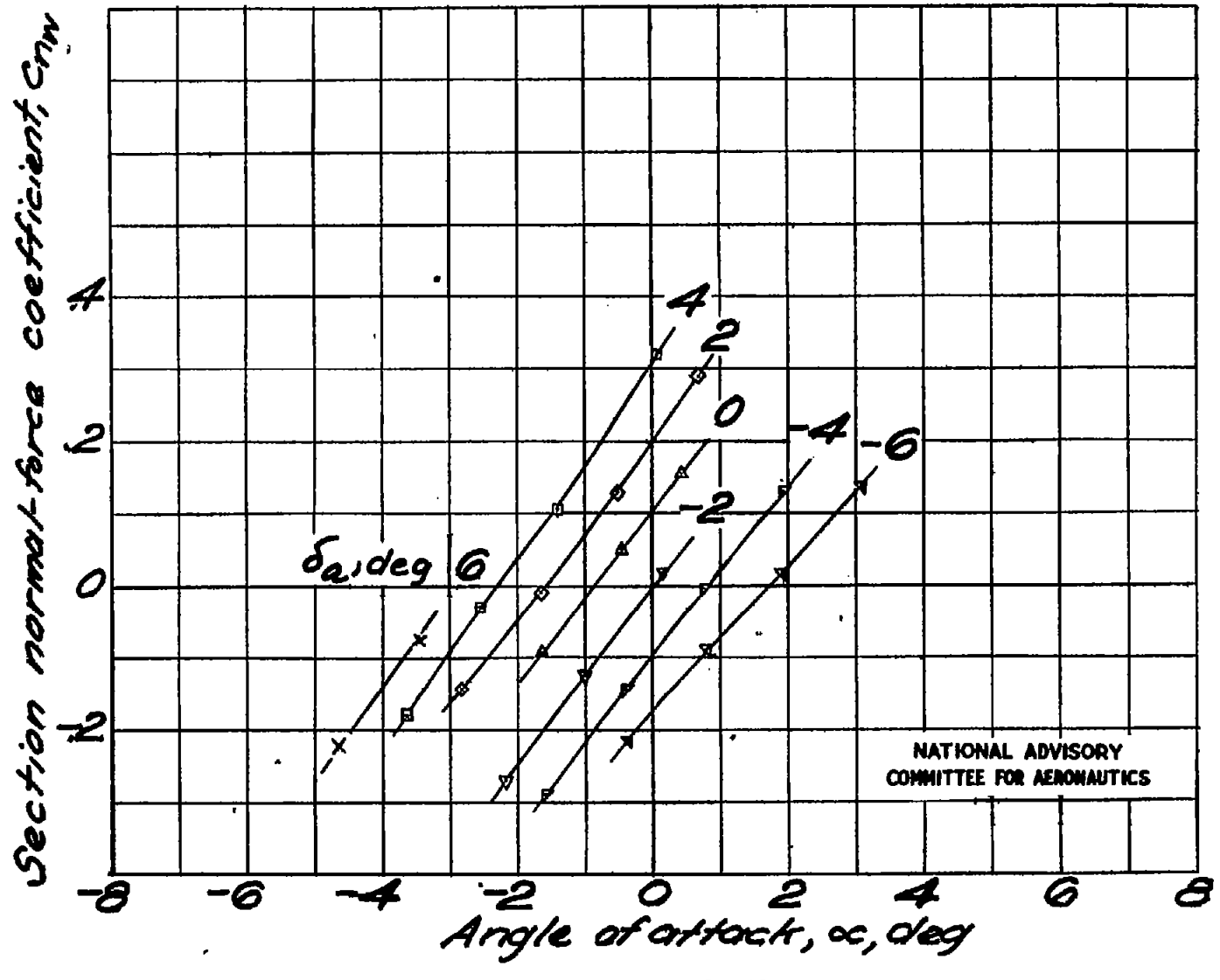

(f) M = 0.650.

Figure 2.- Continued.

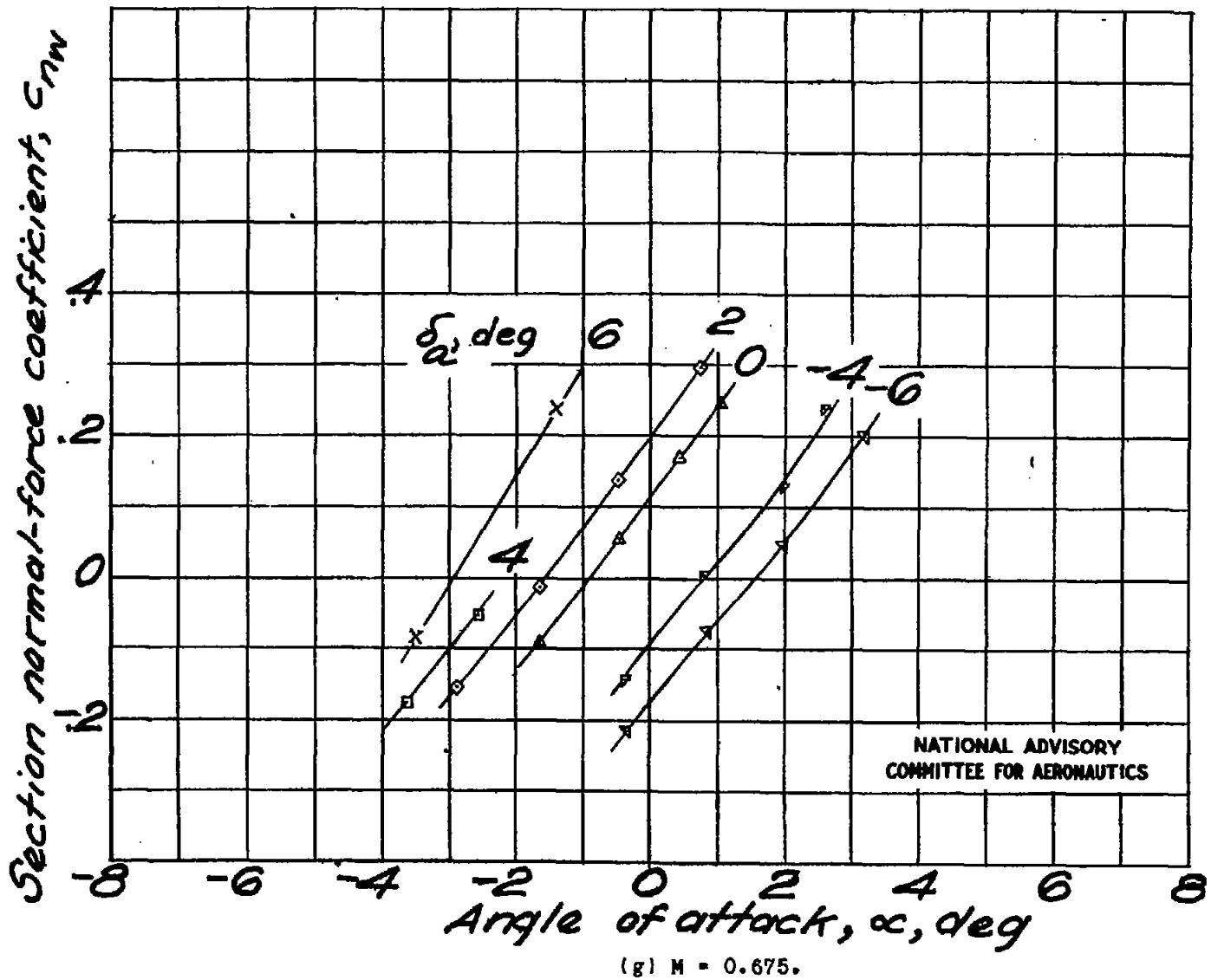

(g) M = 0.675.

Figure 2.- Continued.

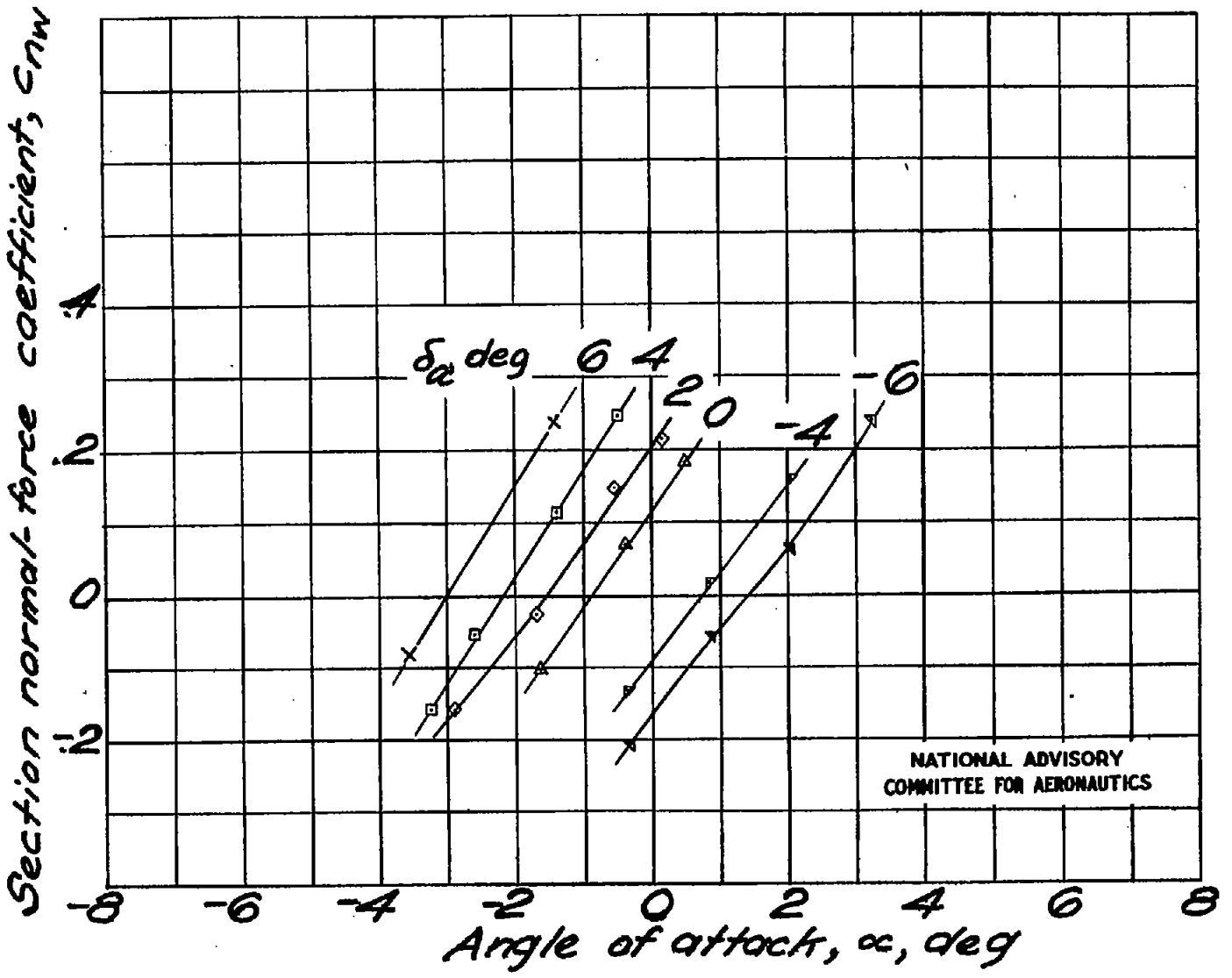

(h) M = 0.700.

Figure 2.- Continued.

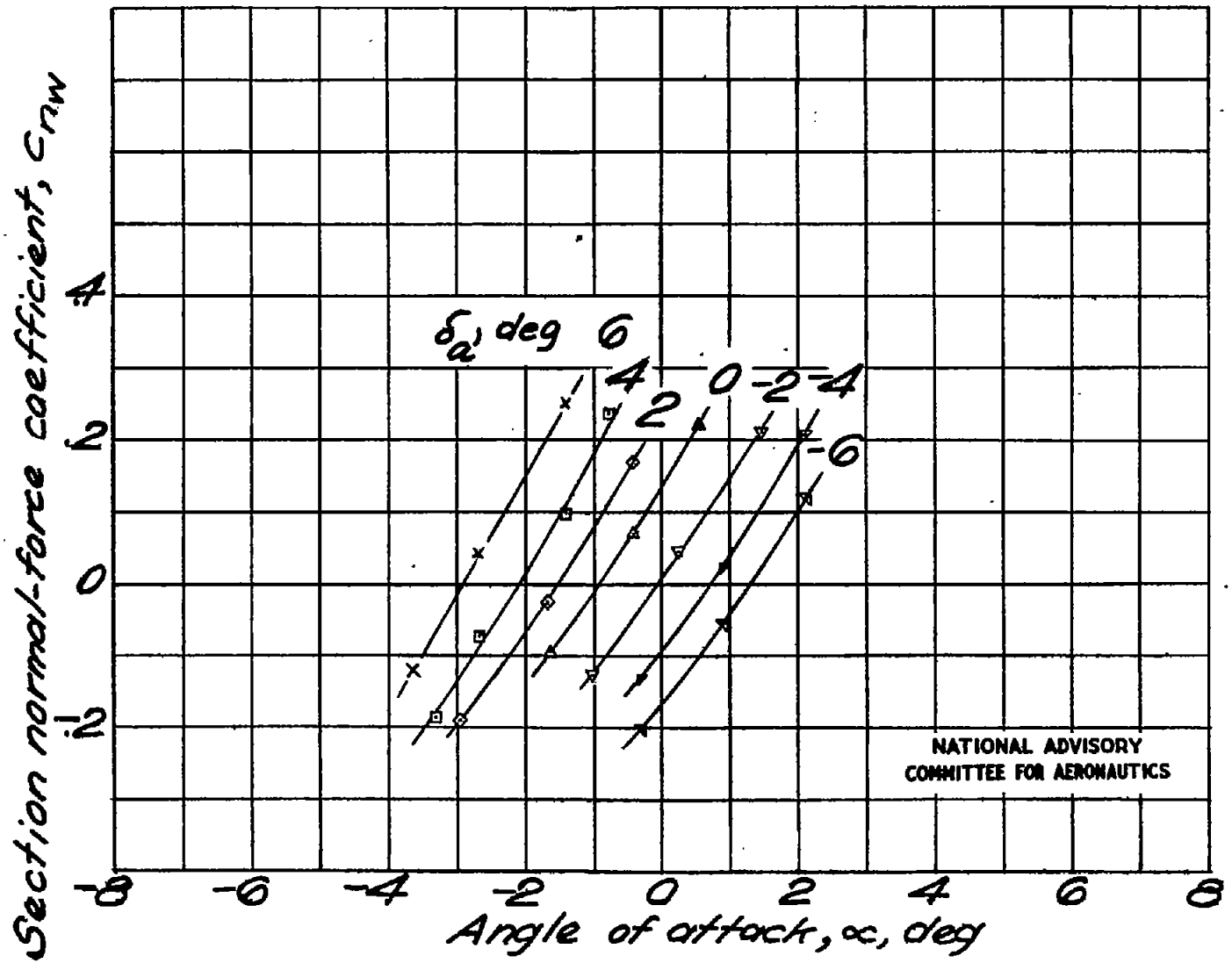

(i) M = 0.725.

Figure 2.- Continued.

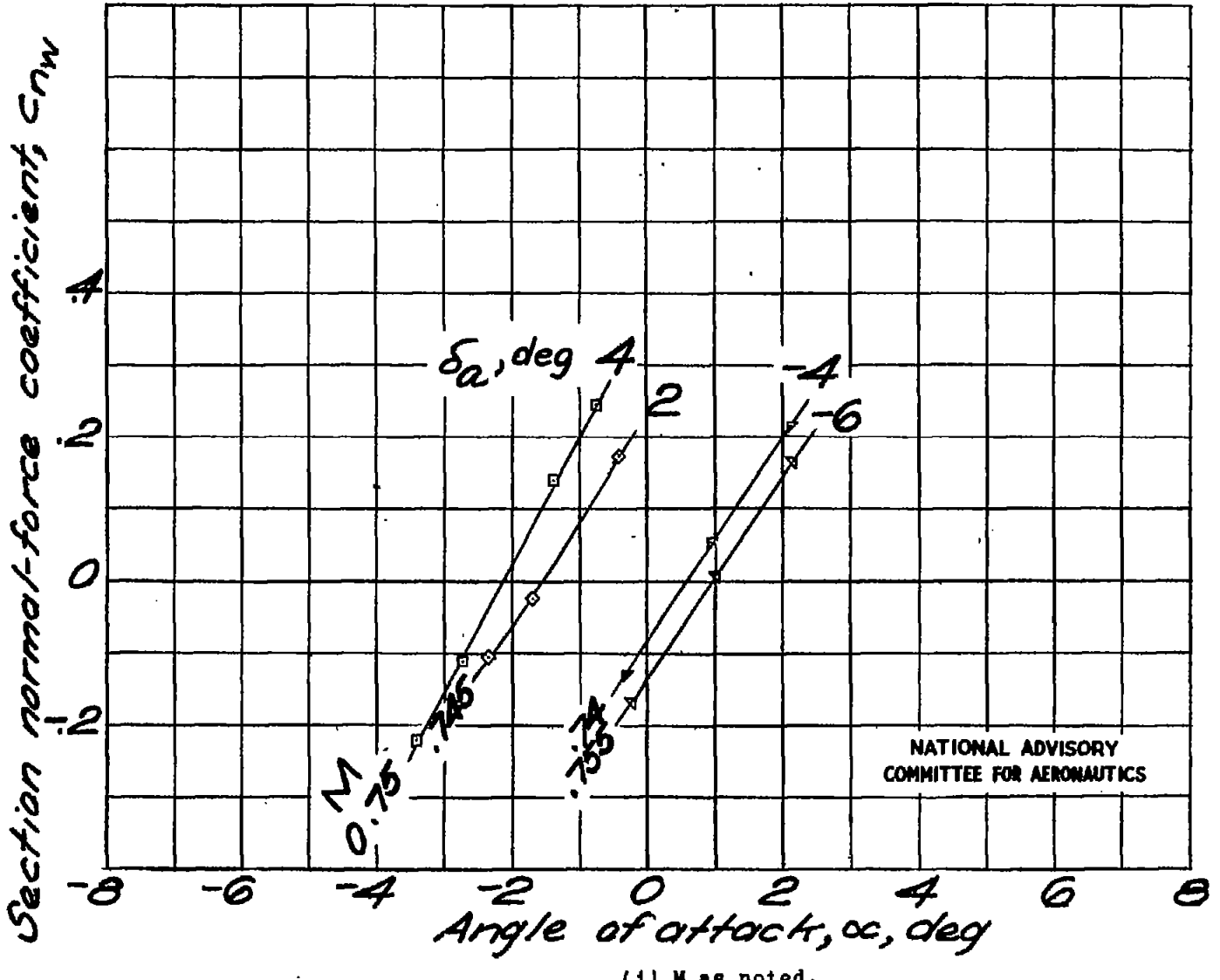

(j) M as noted.

Figure 2.- Continued.

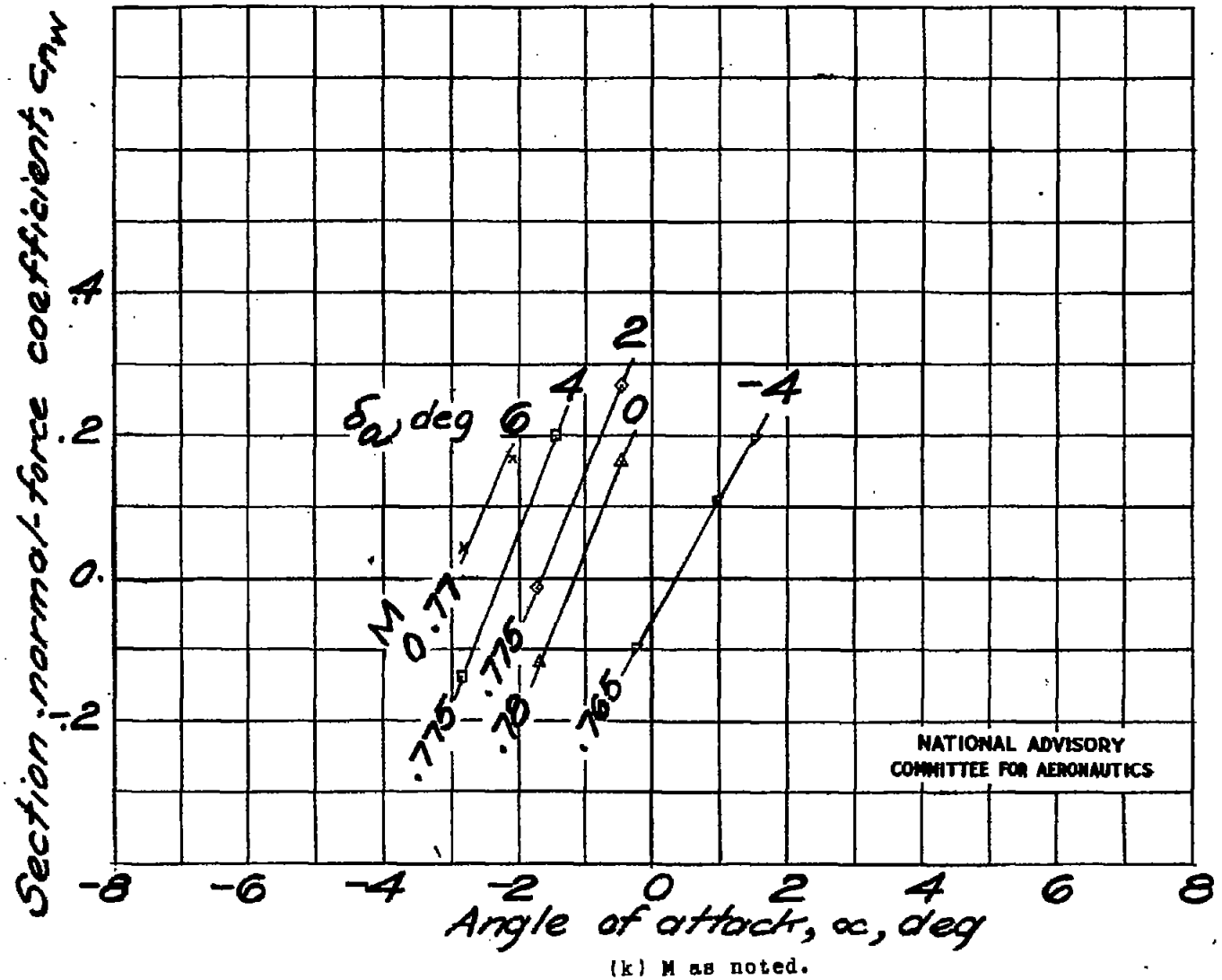

(k) M as noted.

Figure 2.- Concluded.

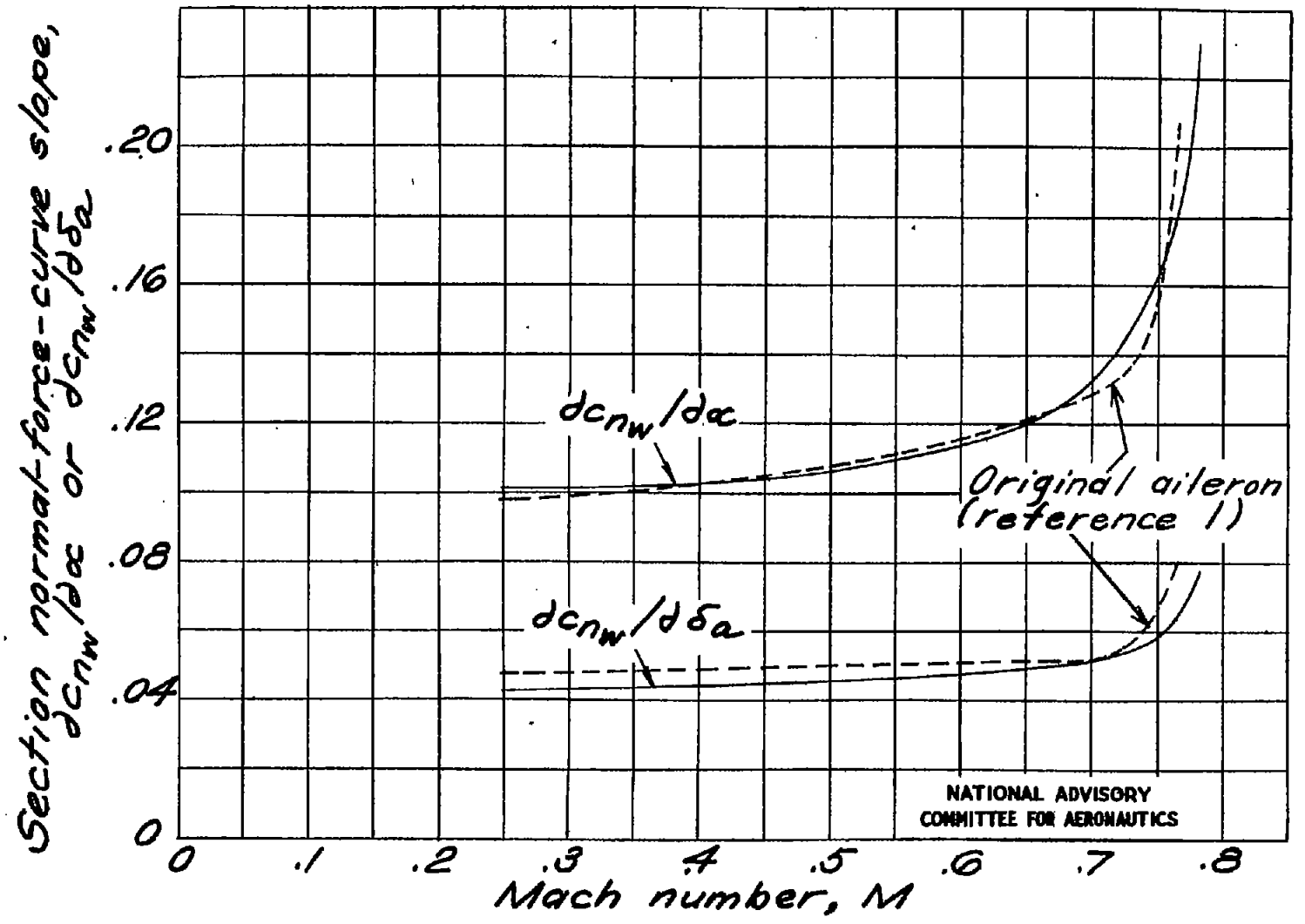

Figure 3.- Effect of compressibility on normal-force-curve slope $\partial c_{n_w}/\partial \alpha$ at $\delta_a = 0^\circ$ and $\partial c_{n_w}/\partial \delta_a$ at $\alpha = 0^\circ$.

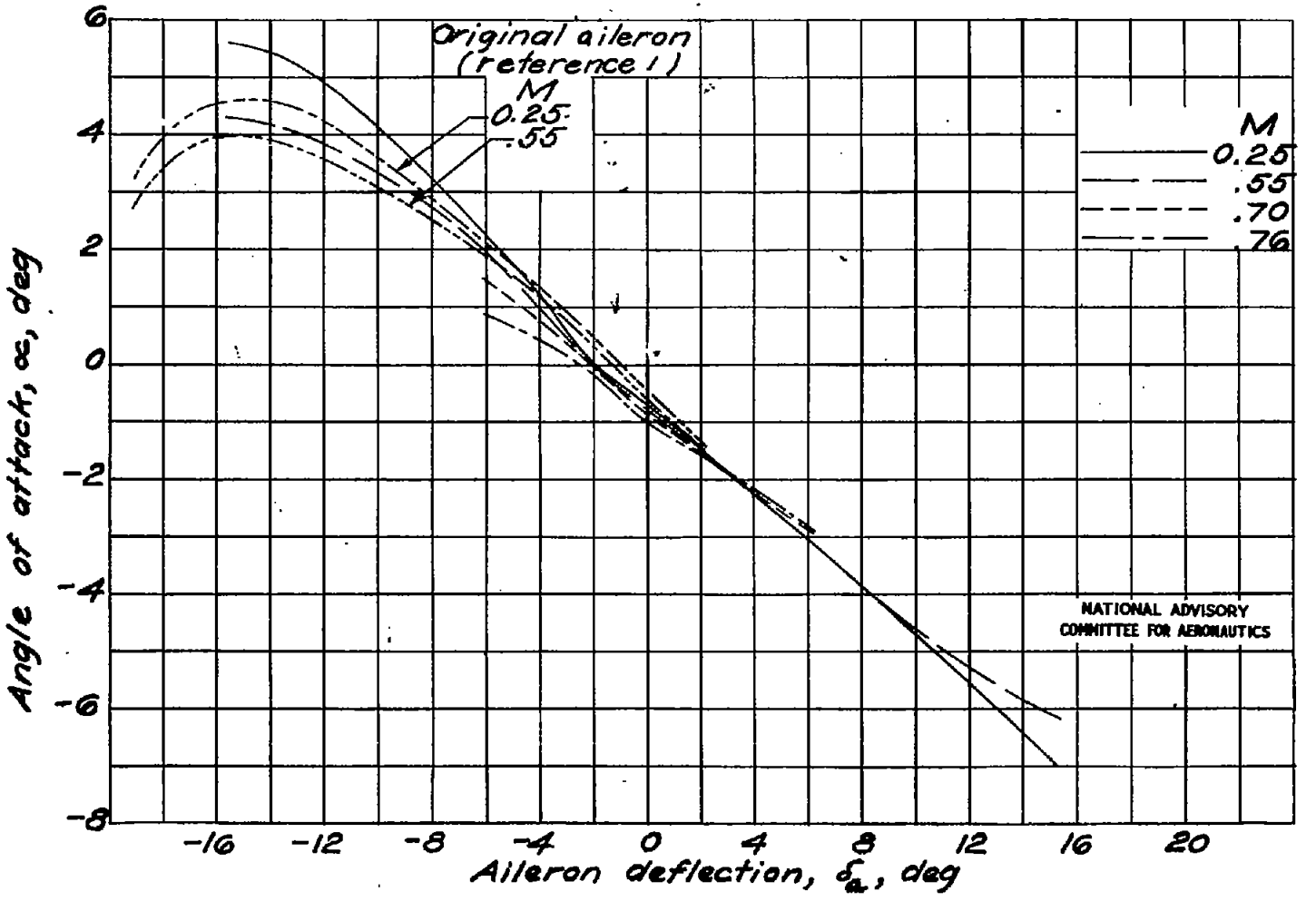

Figure 4.- Angle of attack for a section airfoil normal-force coefficient of 0 against aileron deflection at various Mach numbers.

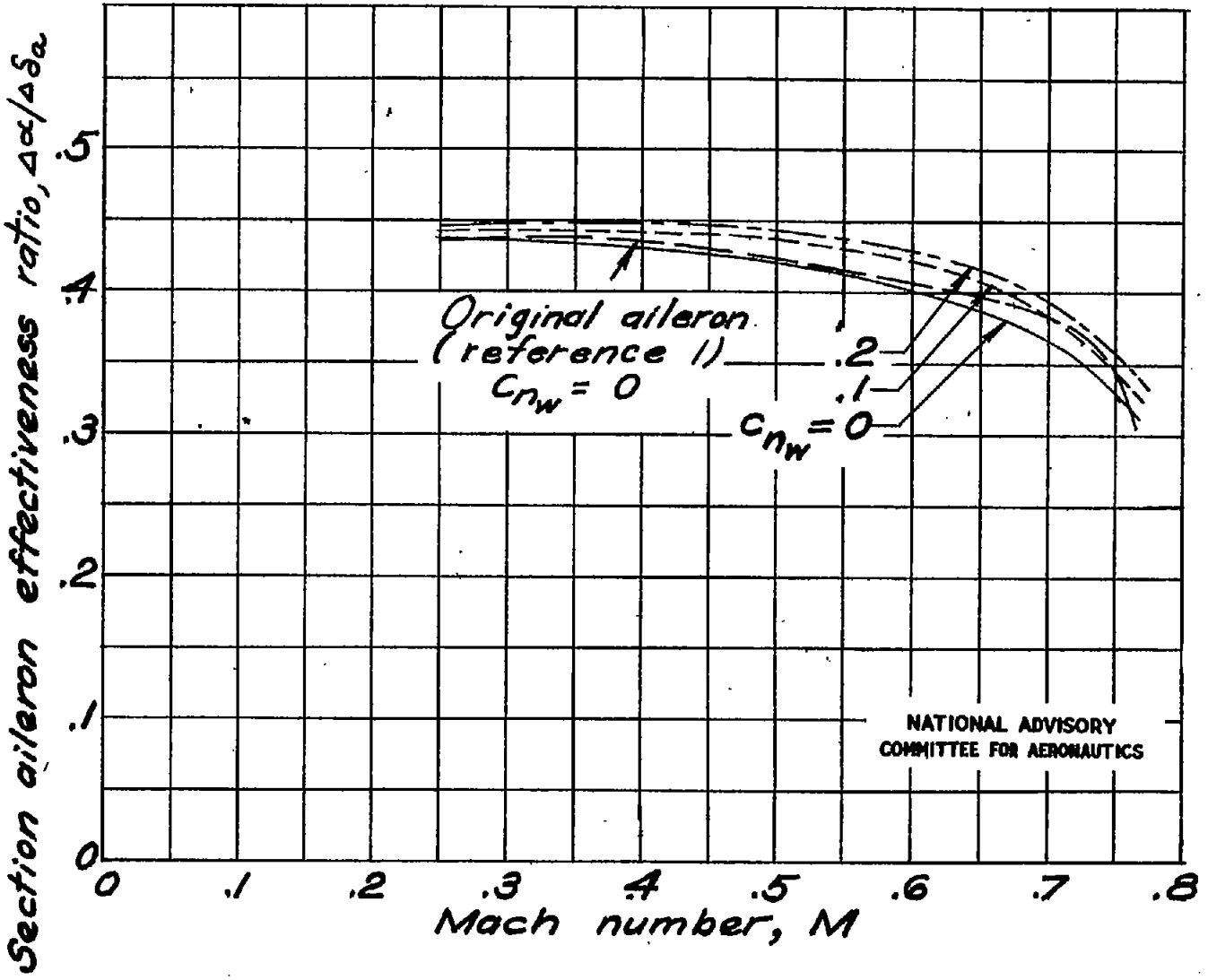

Figure 5.- Section aileron effectiveness for aileron deflections from -6° to 6° against Mach number at various section airfoil normal-force coefficients.

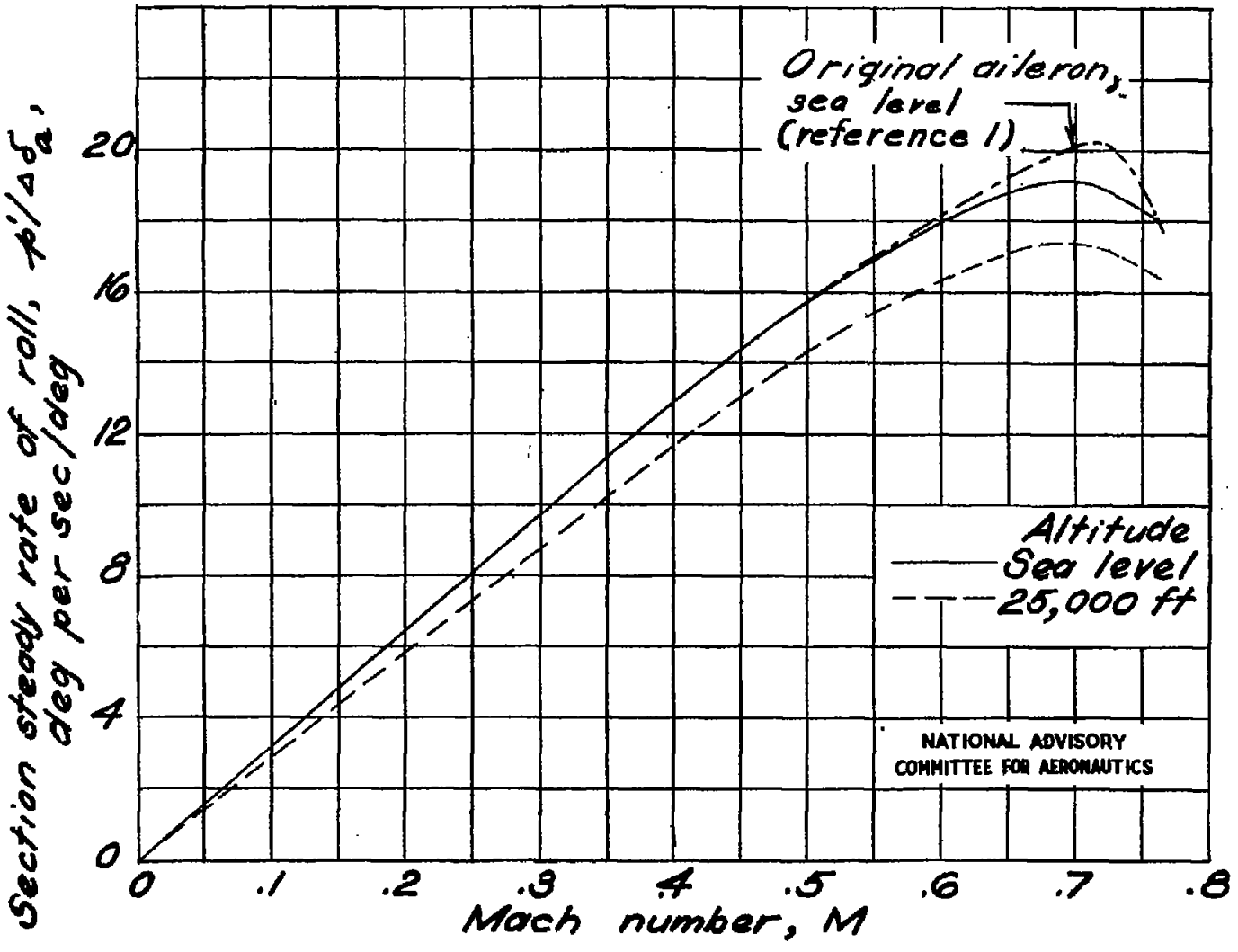

Figure 6.- Section steady rate of roll per degree deflection of single aileron against Mach number. $c_{n_w} = 0$.

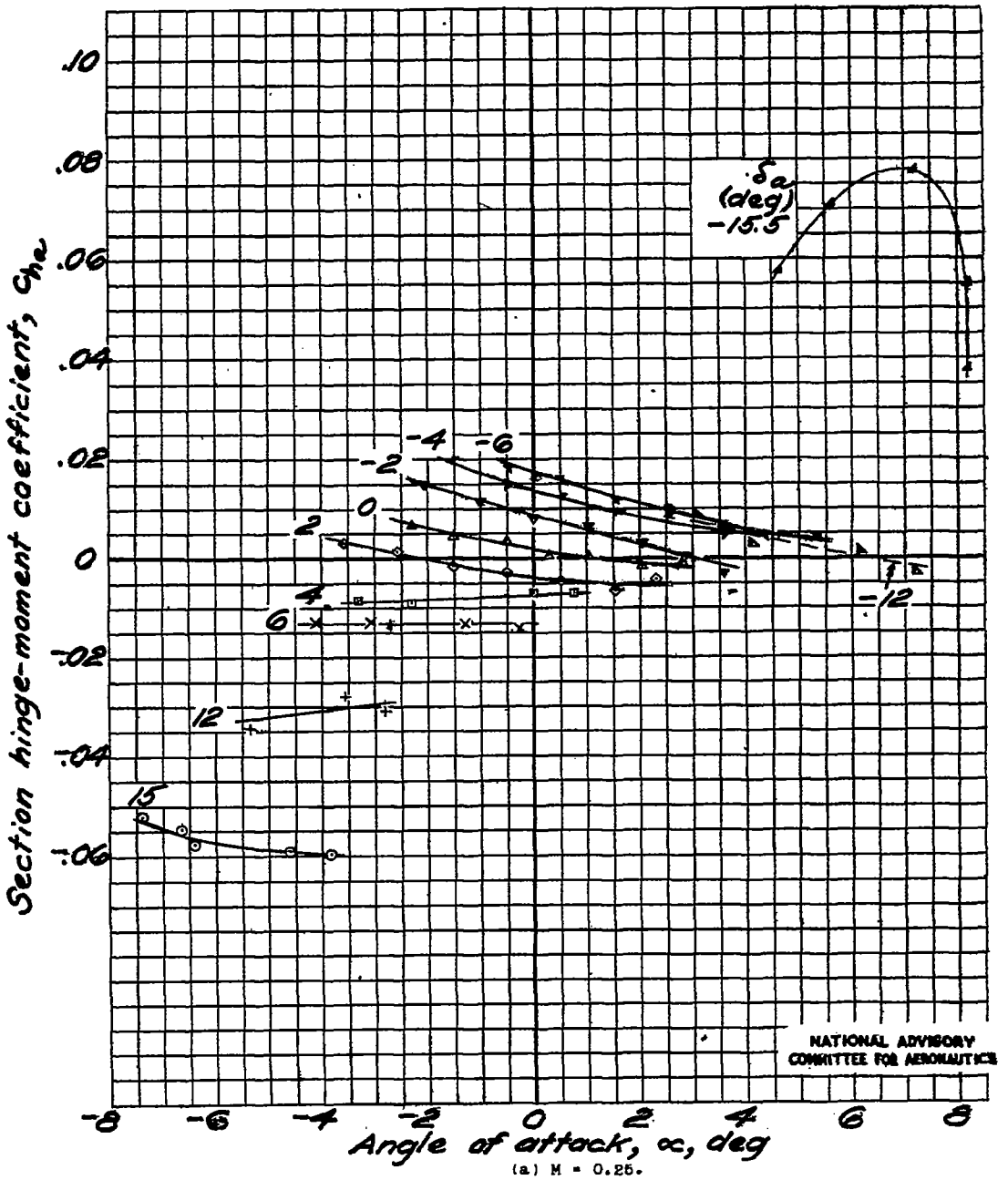

(a) M = 0.25.

Figure 7.- Section aileron hinge-moment coefficient against angle of attack at various aileron deflections.

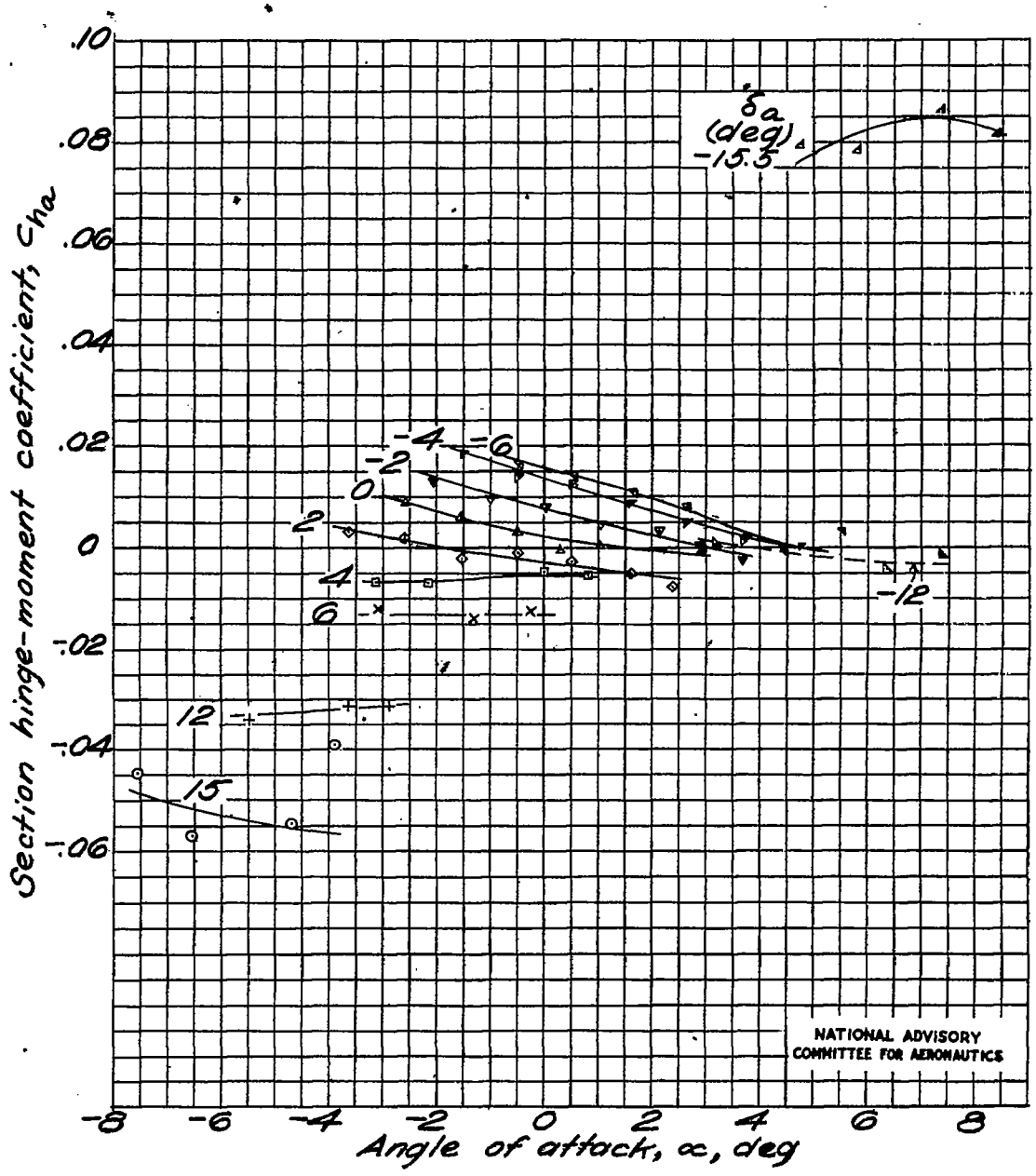

(b) M = 0.350.

Figure 7.- Continued.

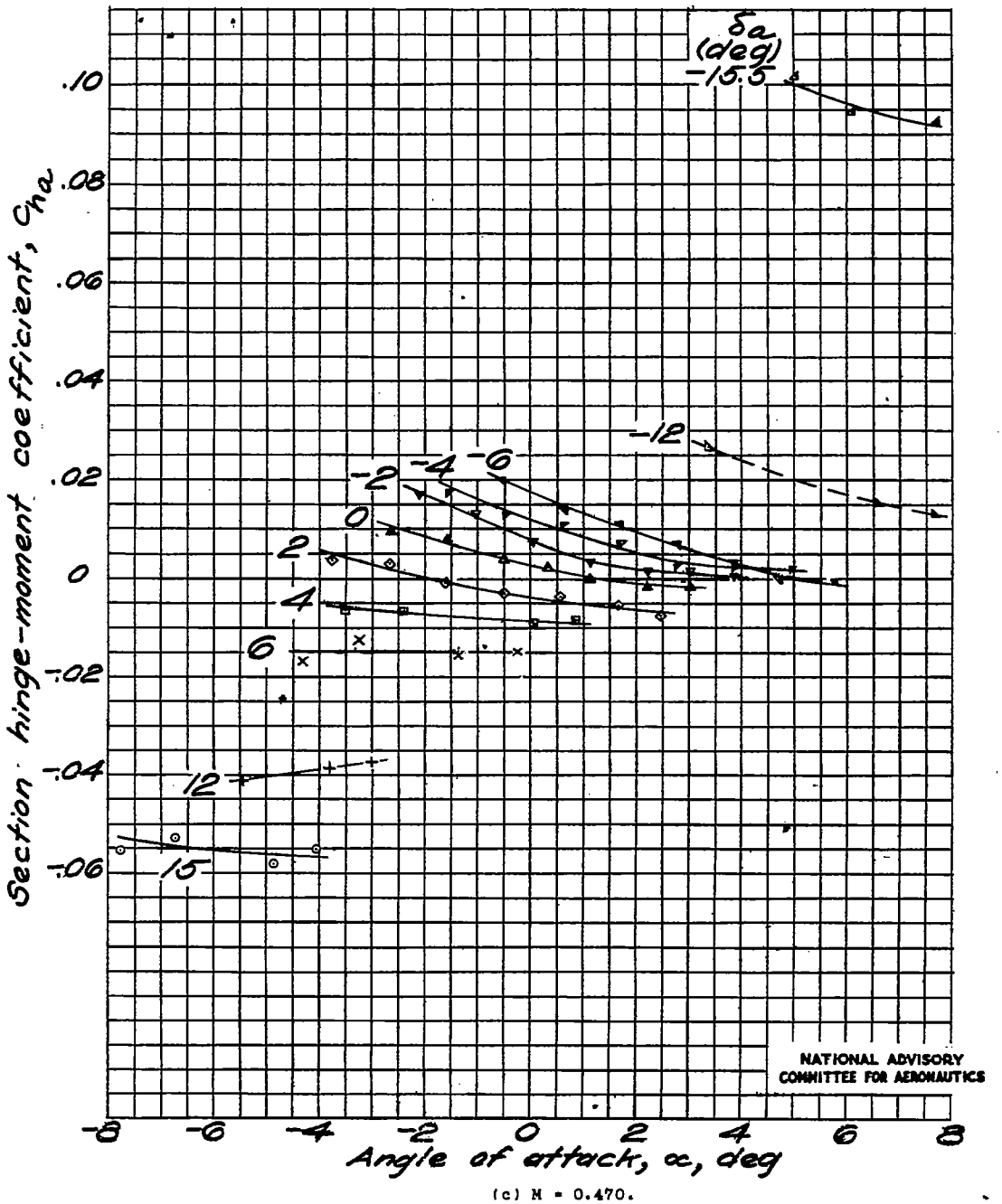

(c) M = 0.470.

Figure 7.- Continued.

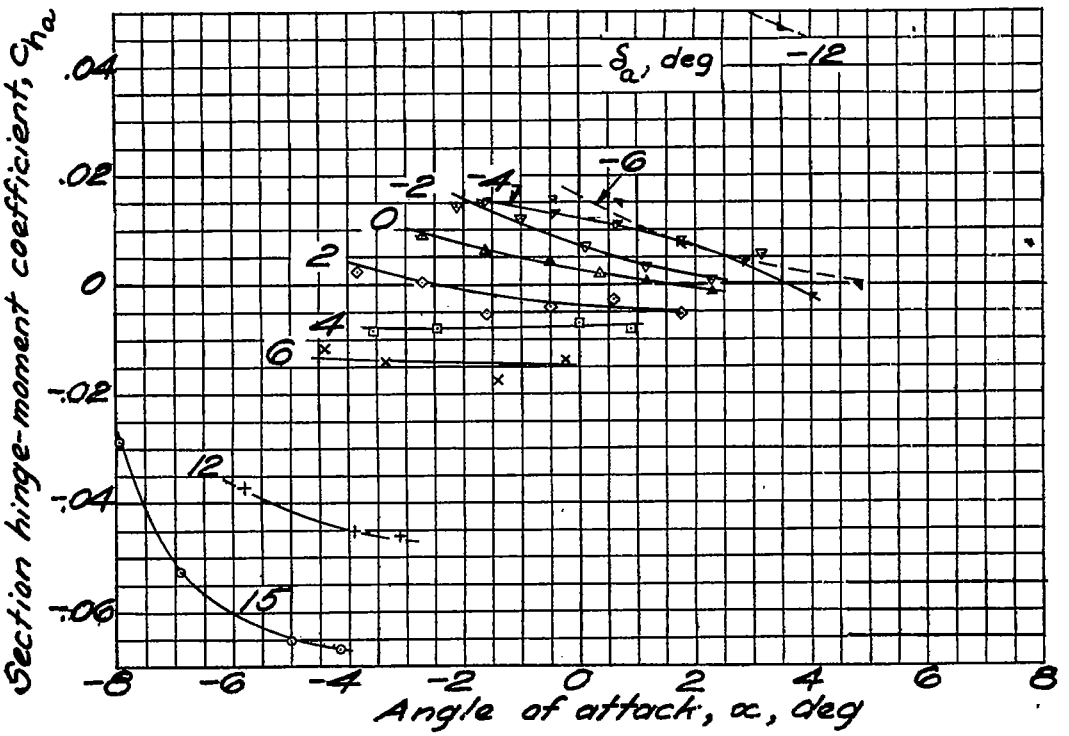

(d) M = 0.550.

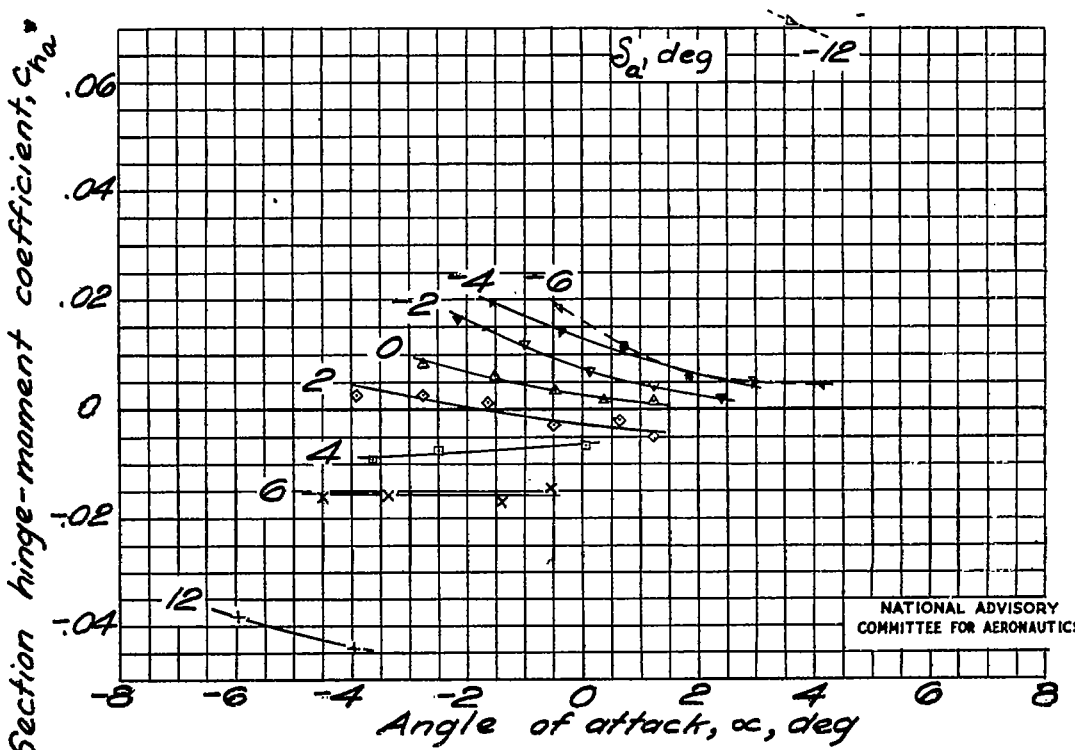

(e) M = 0.600.

Figure 7.- Continued.

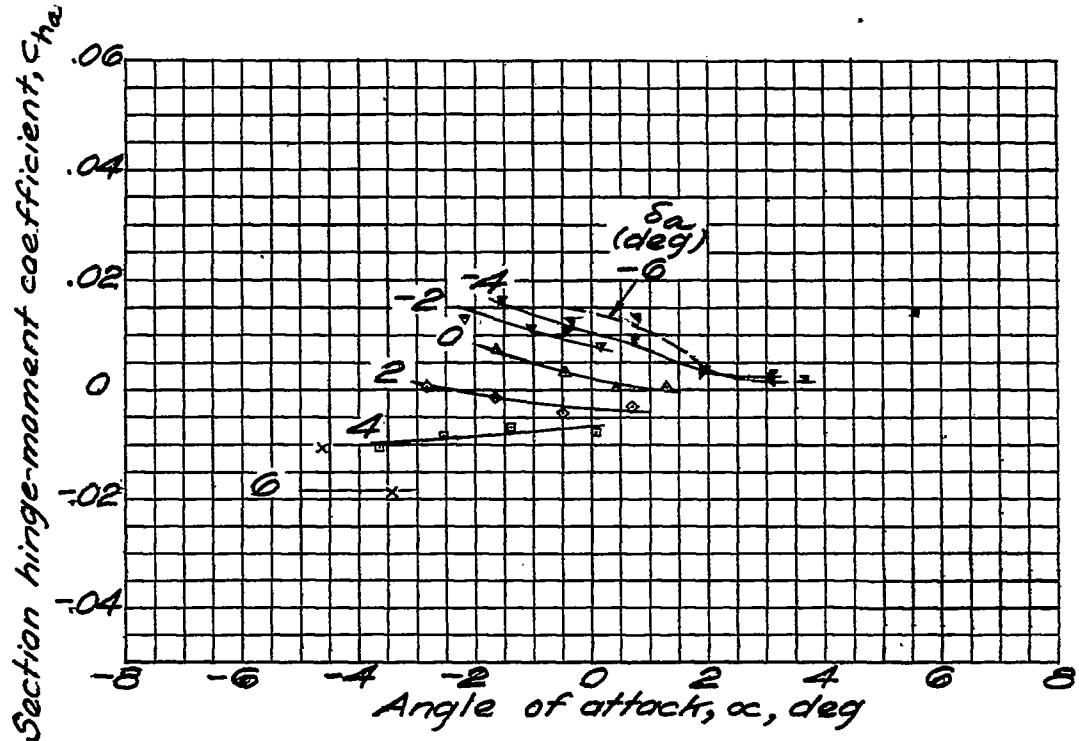

(f) M = 0.650.

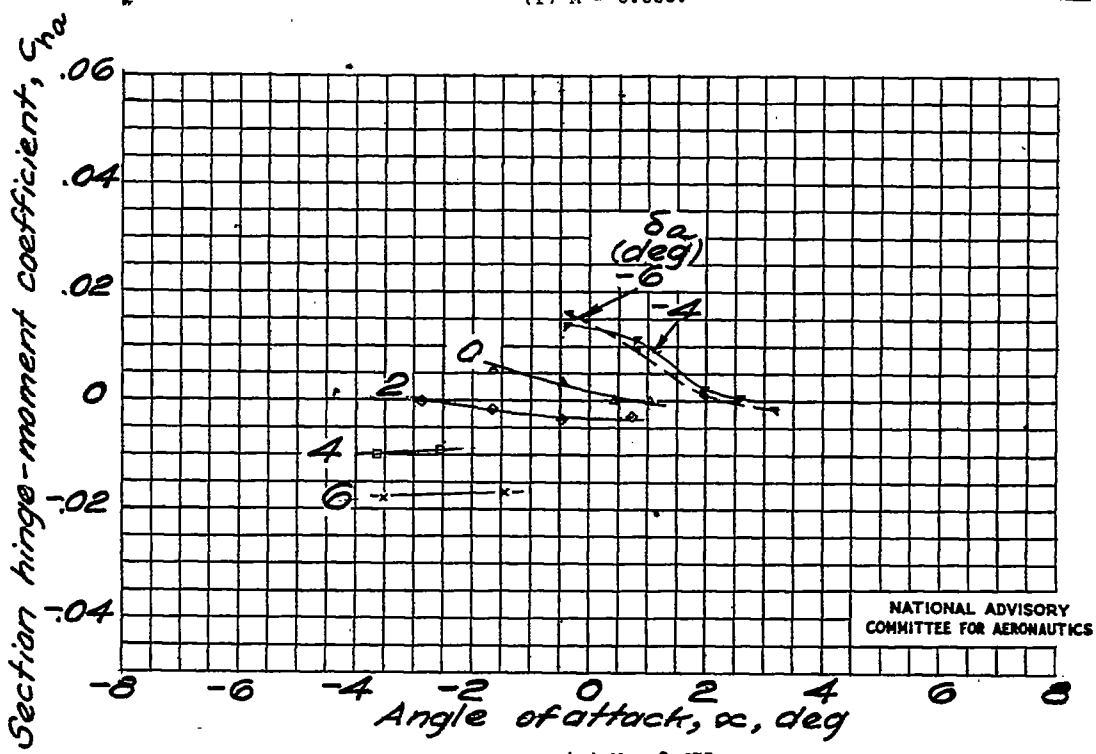

(g) M = 0.675.

Figure 7.- Continued.

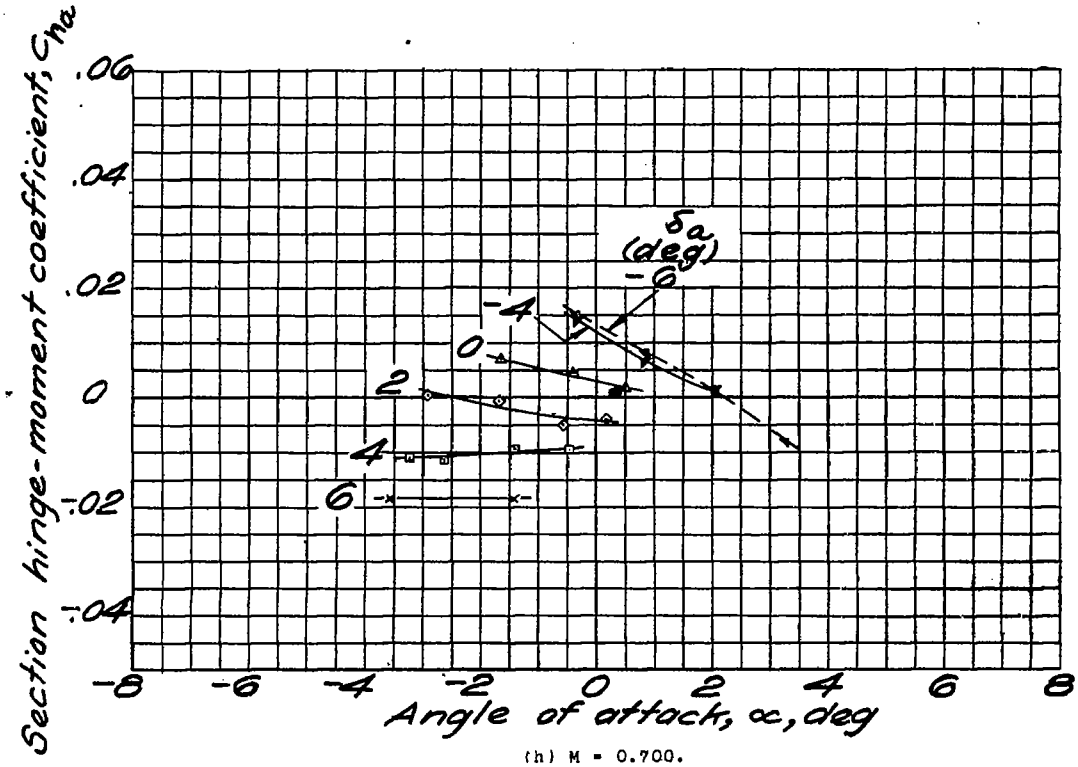

(h) M = 0.700.

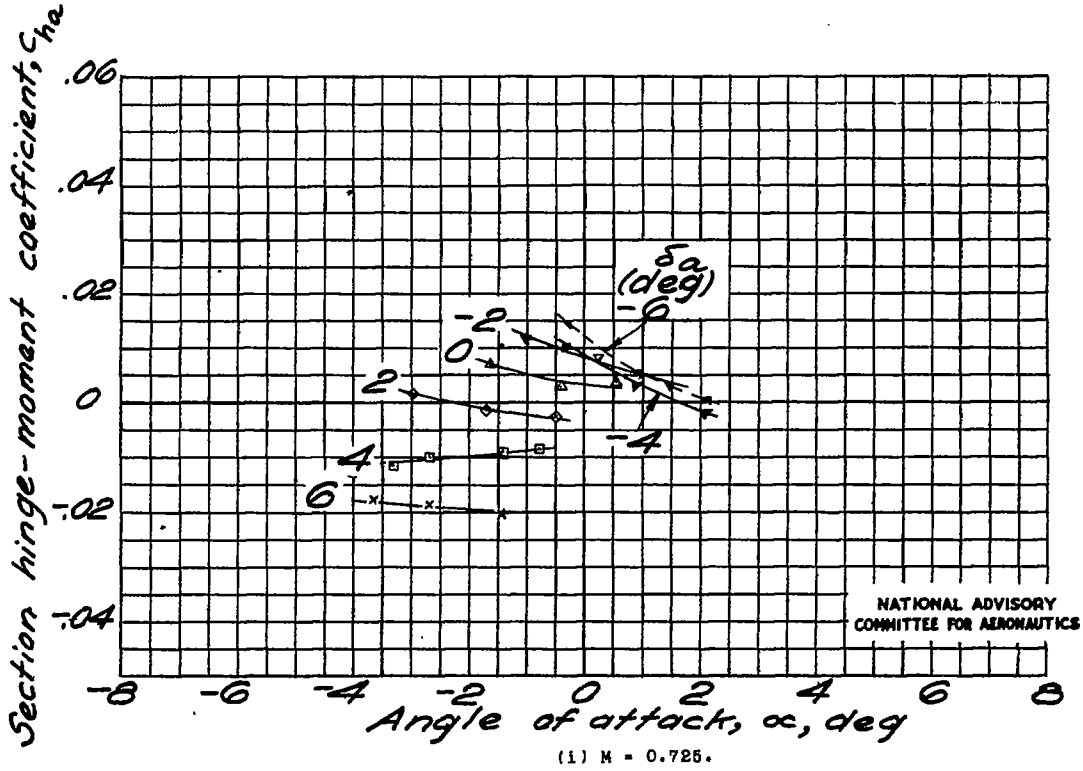

(i) M = 0.725.

Figure 7.- Continued.

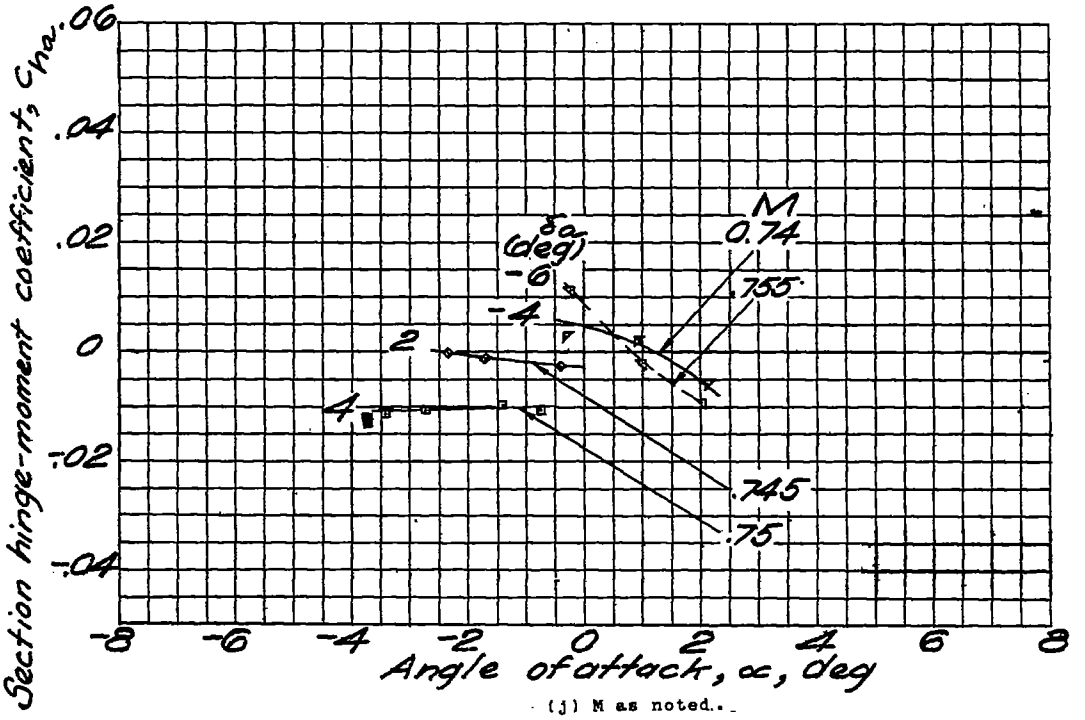

(j) M as noted.

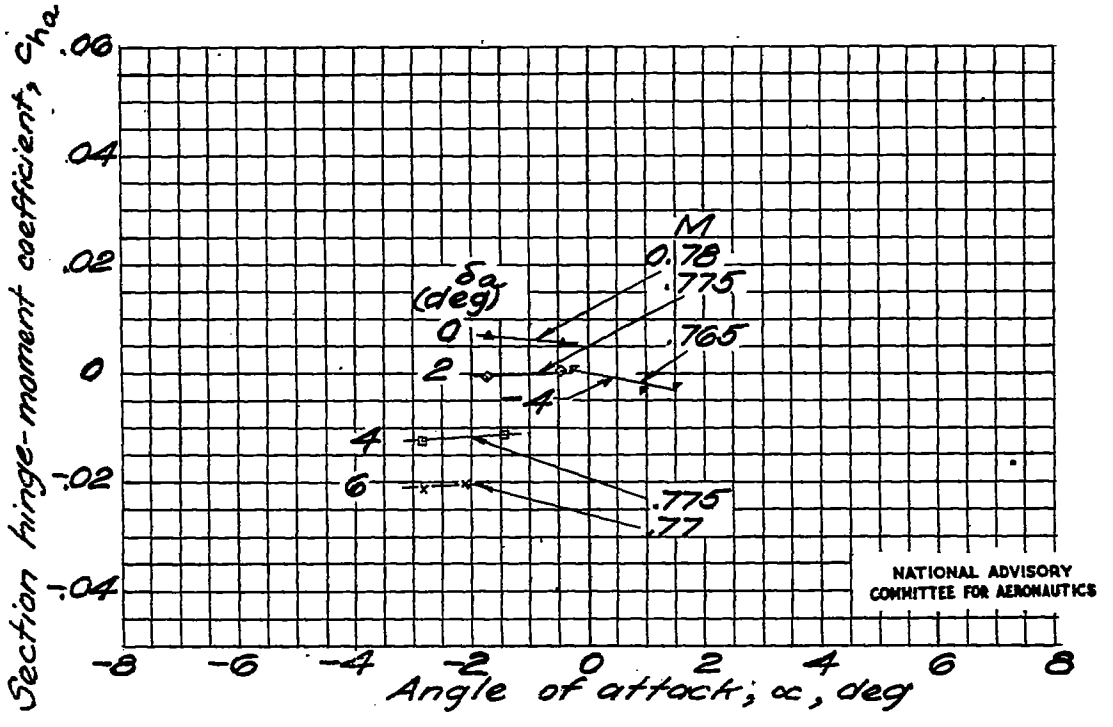

(k) M as noted.

Figure 7.- Concluded.

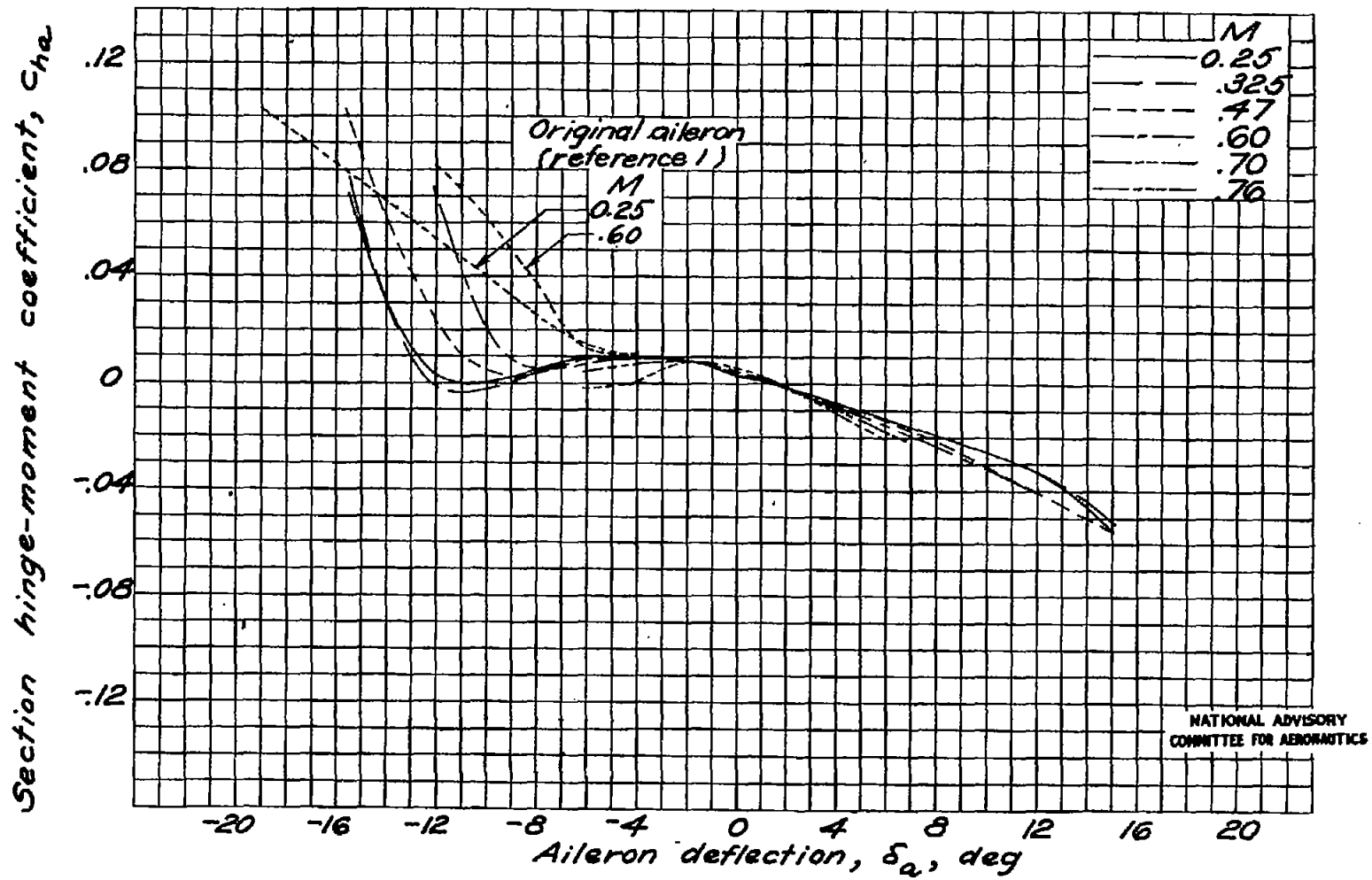

(a) $c_{n_w} = 0$.

Figure 8.- Section aileron hinge-moment coefficient against aileron deflection at various Mach numbers.

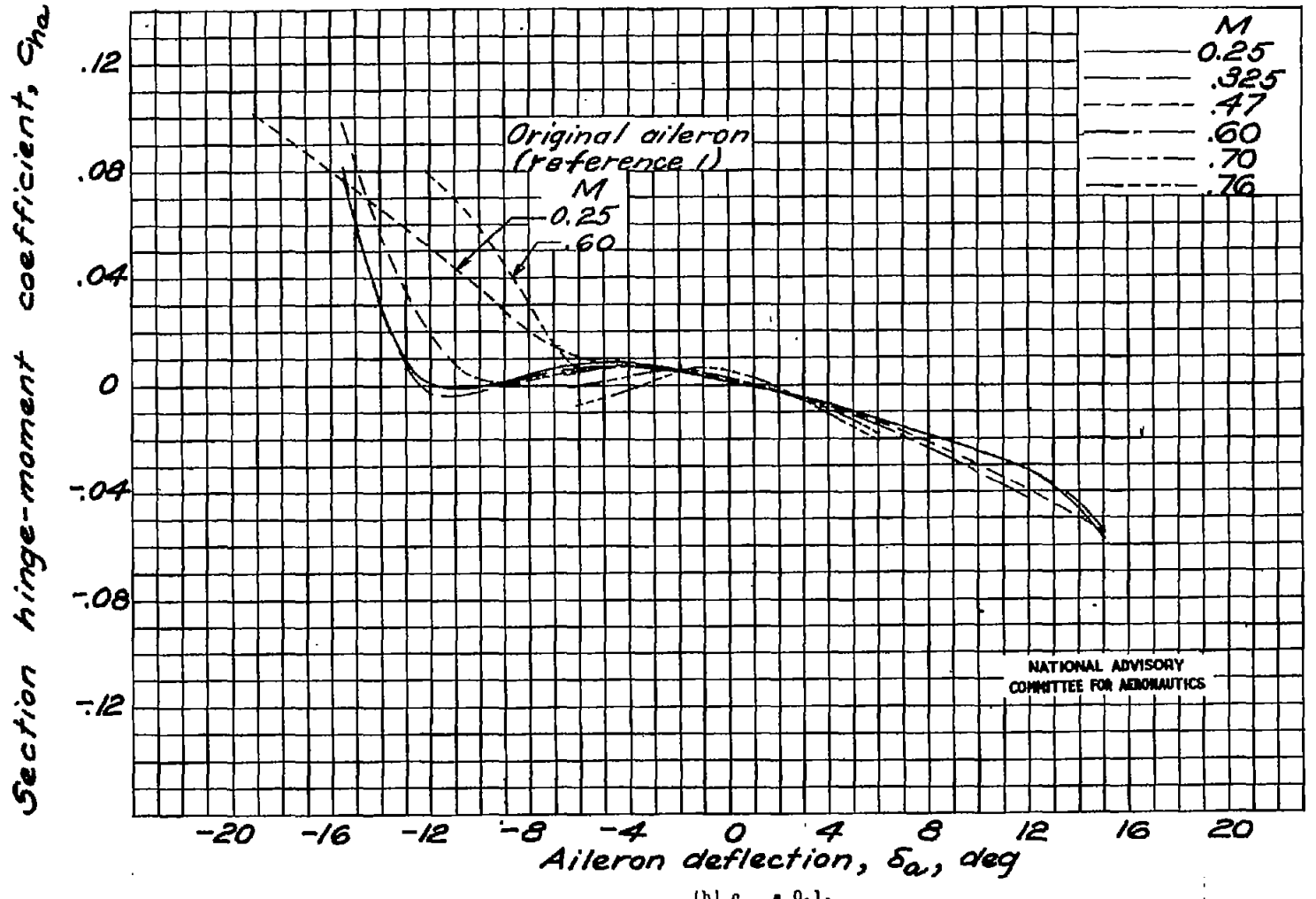

(b) $c_{n_w} = 0.1$.

Figure 8.- Continued.

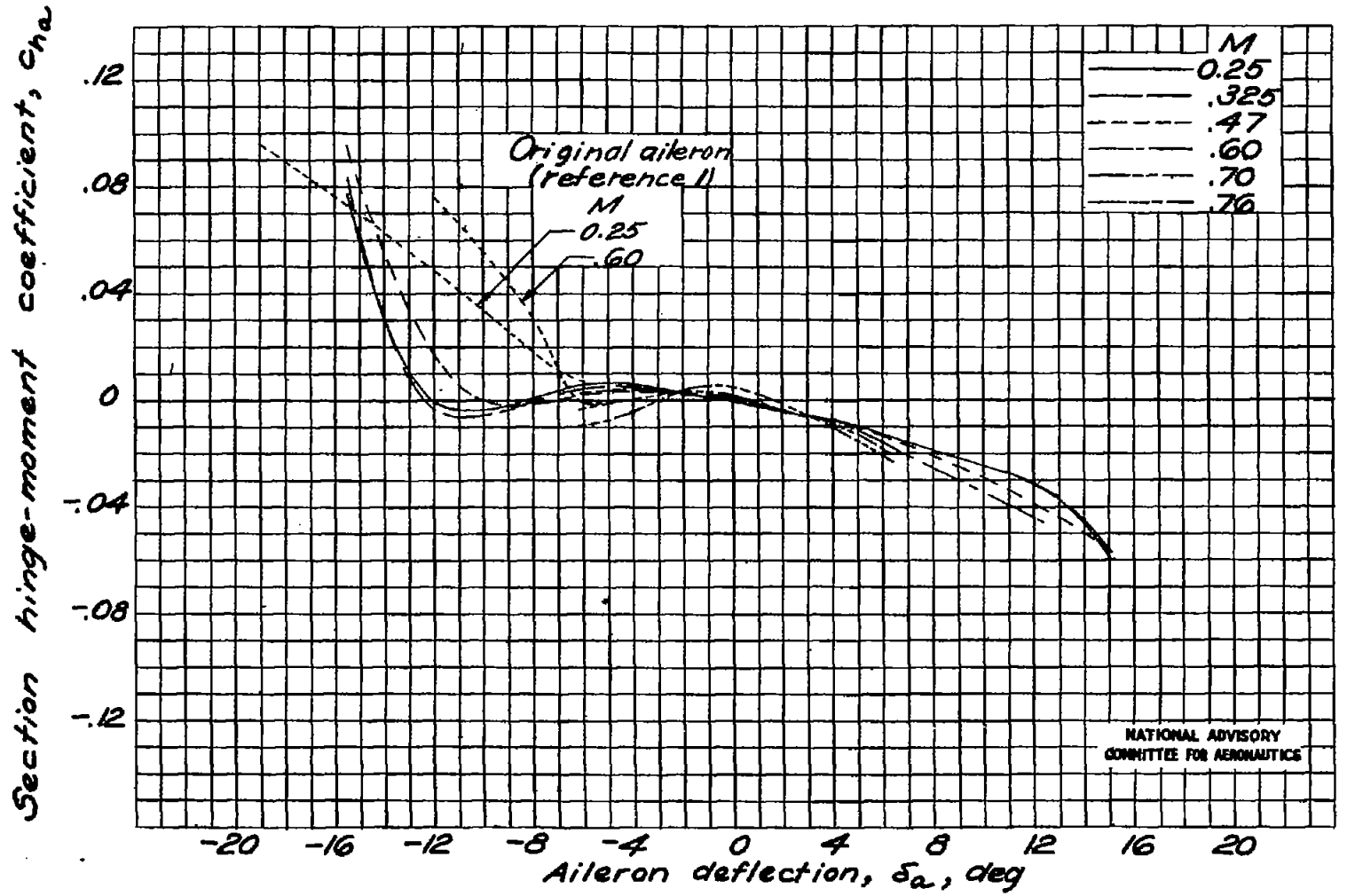

(c) $c_{n_w} = 0.2$.

Figure 8.- Concluded.

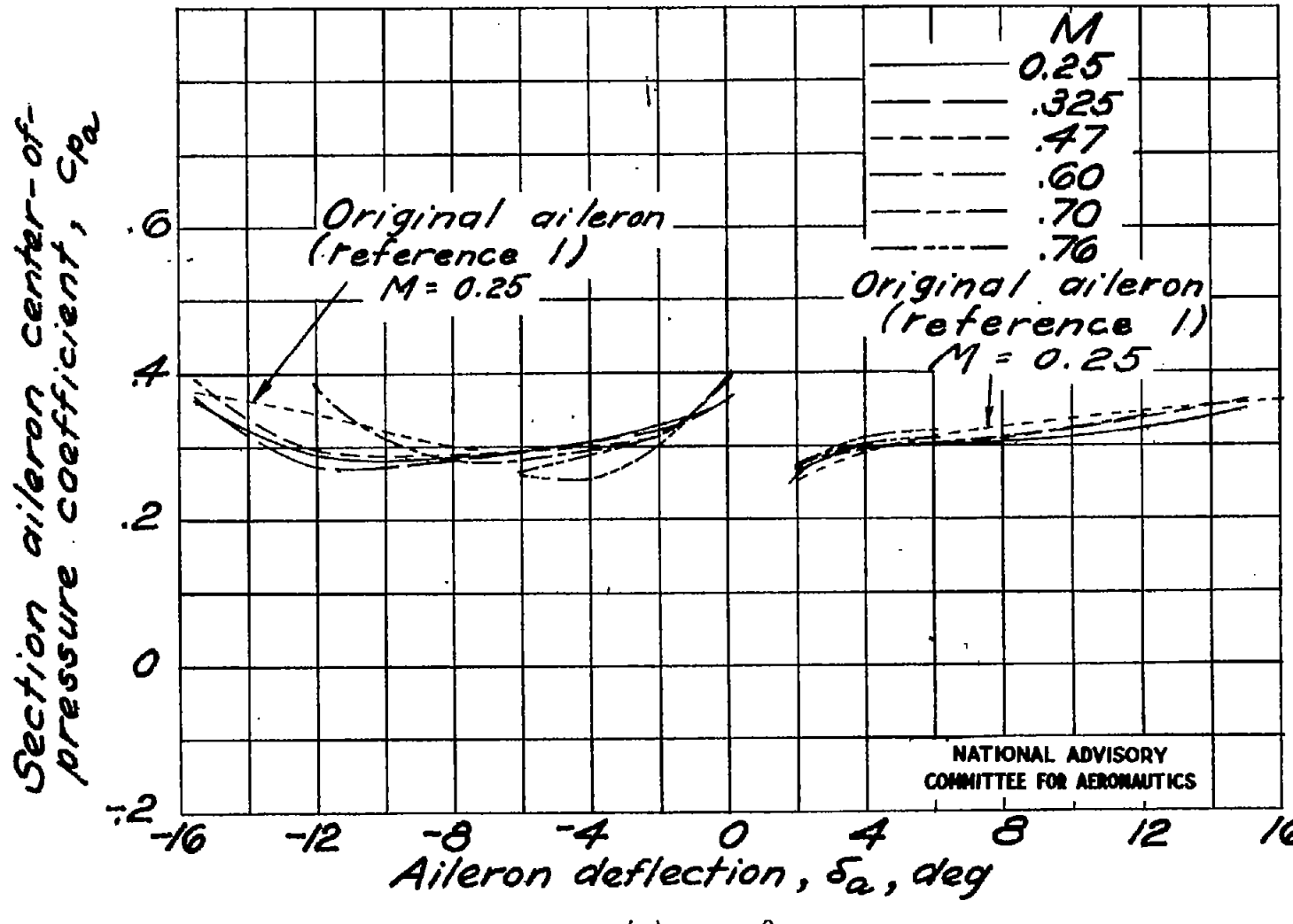

(a) $c_{n_w} = 0$.

Figure 9.- Section aileron center-of-pressure coefficient against aileron deflection at various Mach numbers.

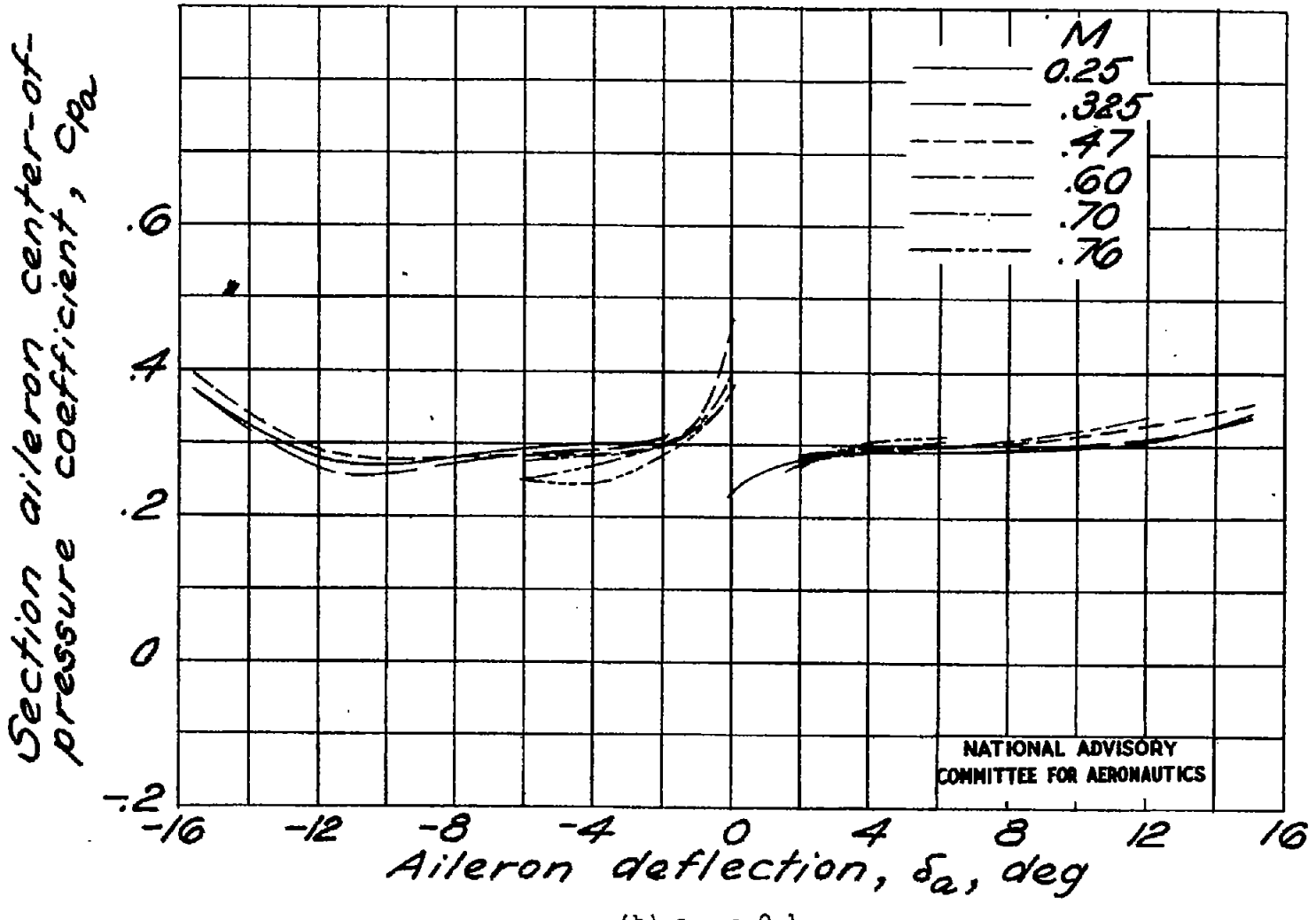

(b) $c_{n_w} = 0.1$.

Figure 9.- Continued.

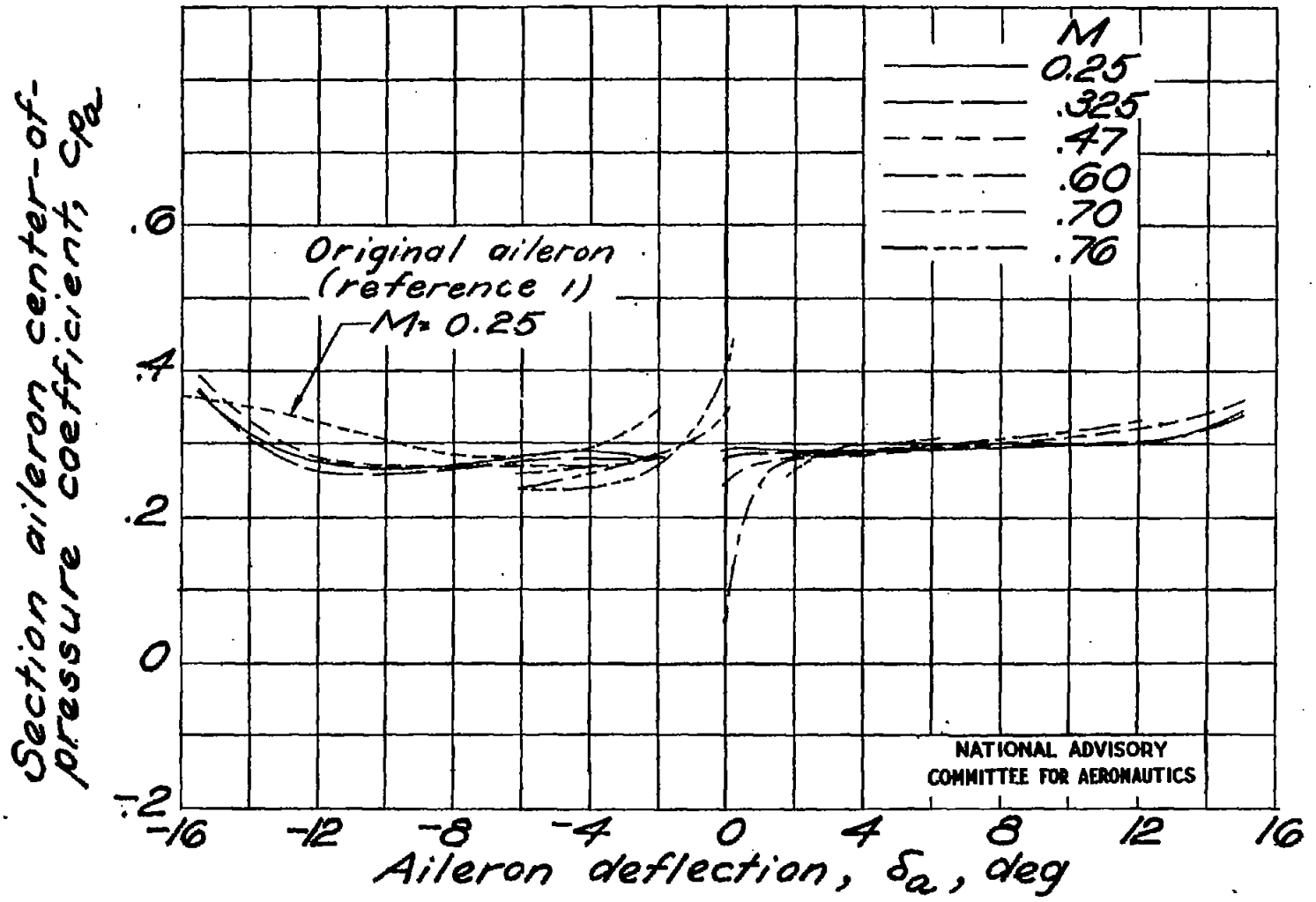

(c) $c_{n_w} = 0.2$.

Figure 9.- Concluded.

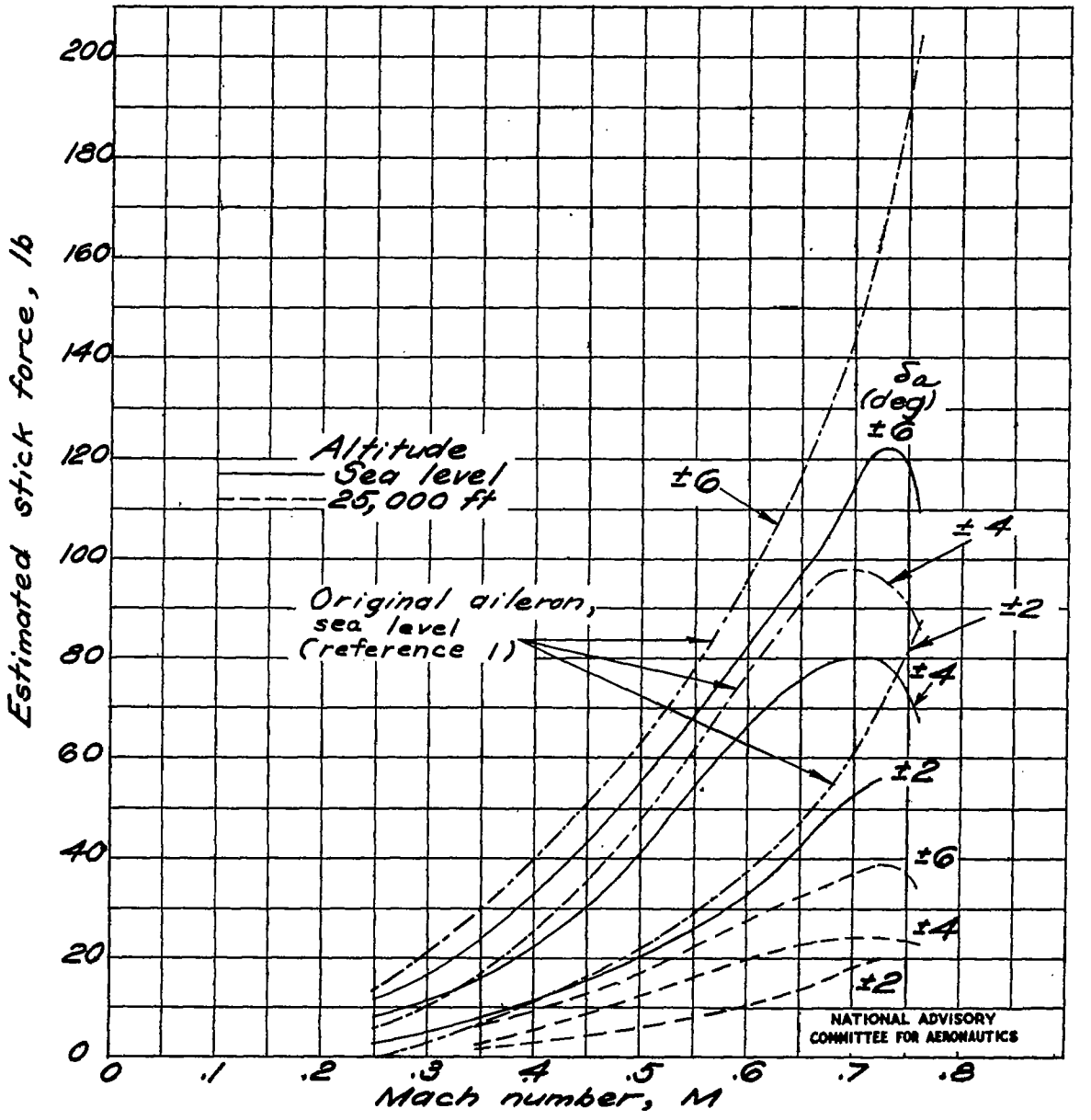

Figure 10.- Estimated aileron stick force for nondifferential aileron deflections and steady rate of roll at two altitudes.

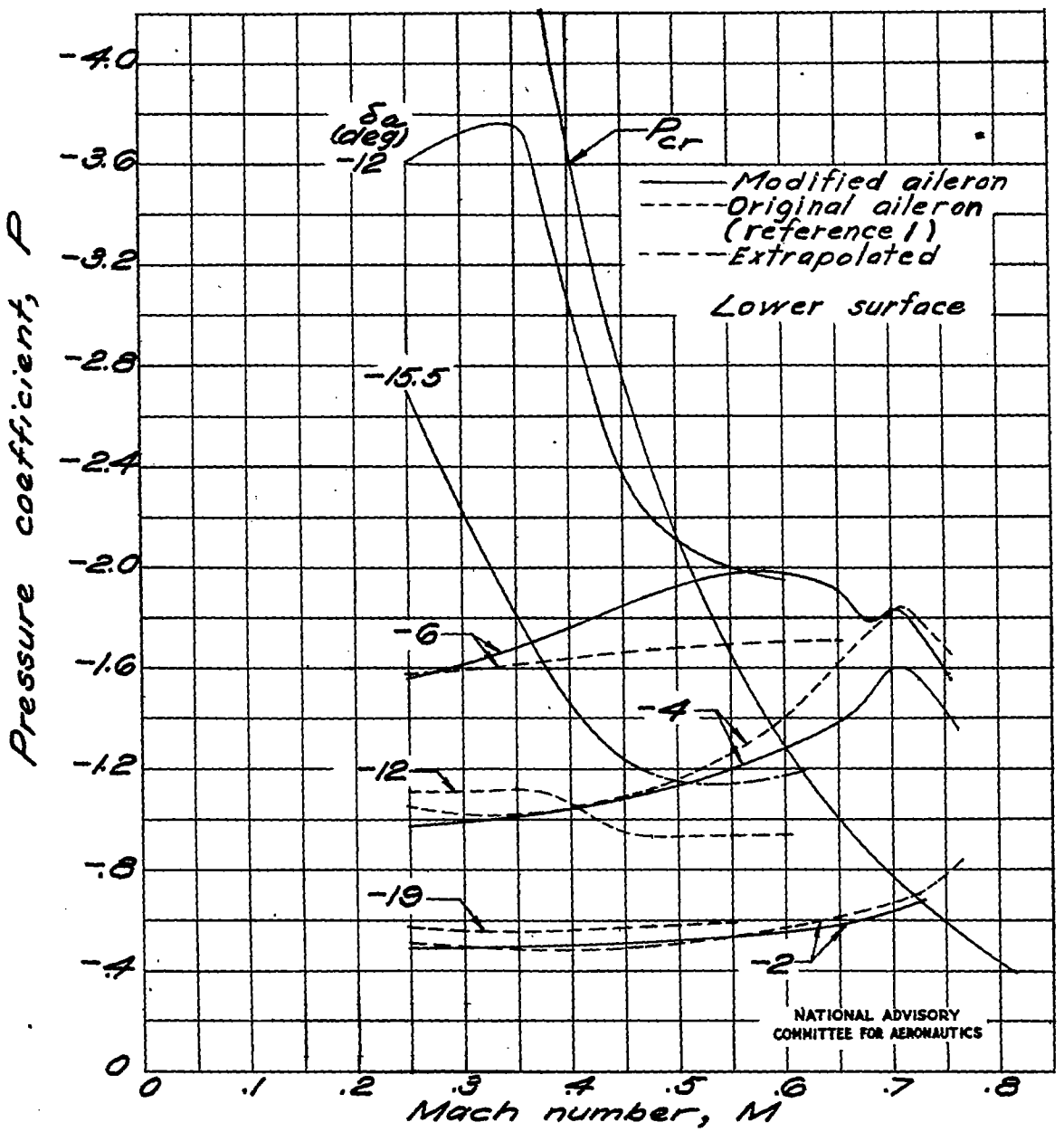

(a) $c_{n_w} = 0$.

Figure 11.- Effect of compressibility and nose shape on peak negative pressure coefficient of aileron.

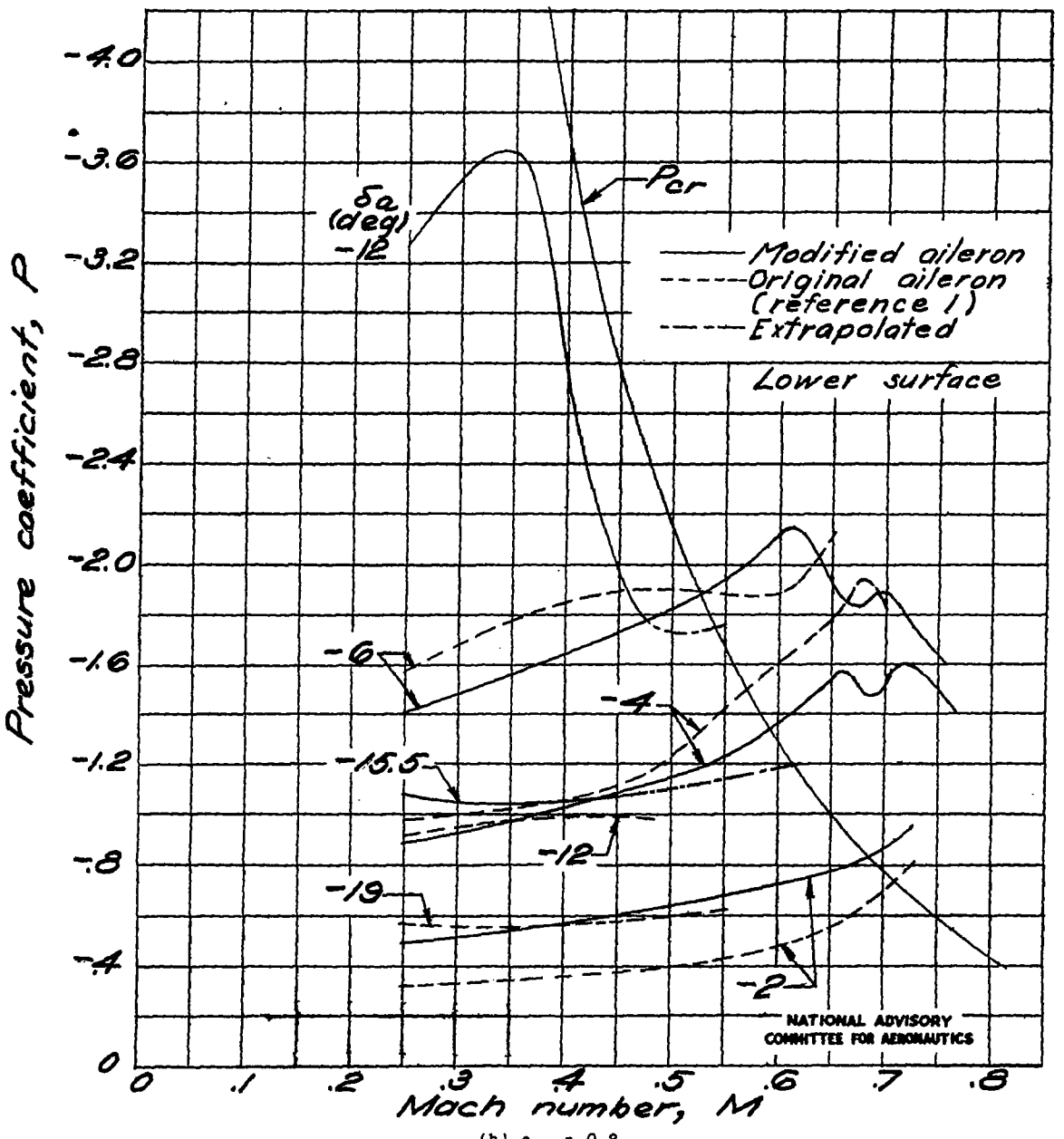

(b) $c_{n_w} = 0.2$.

Figure 11.- Concluded.

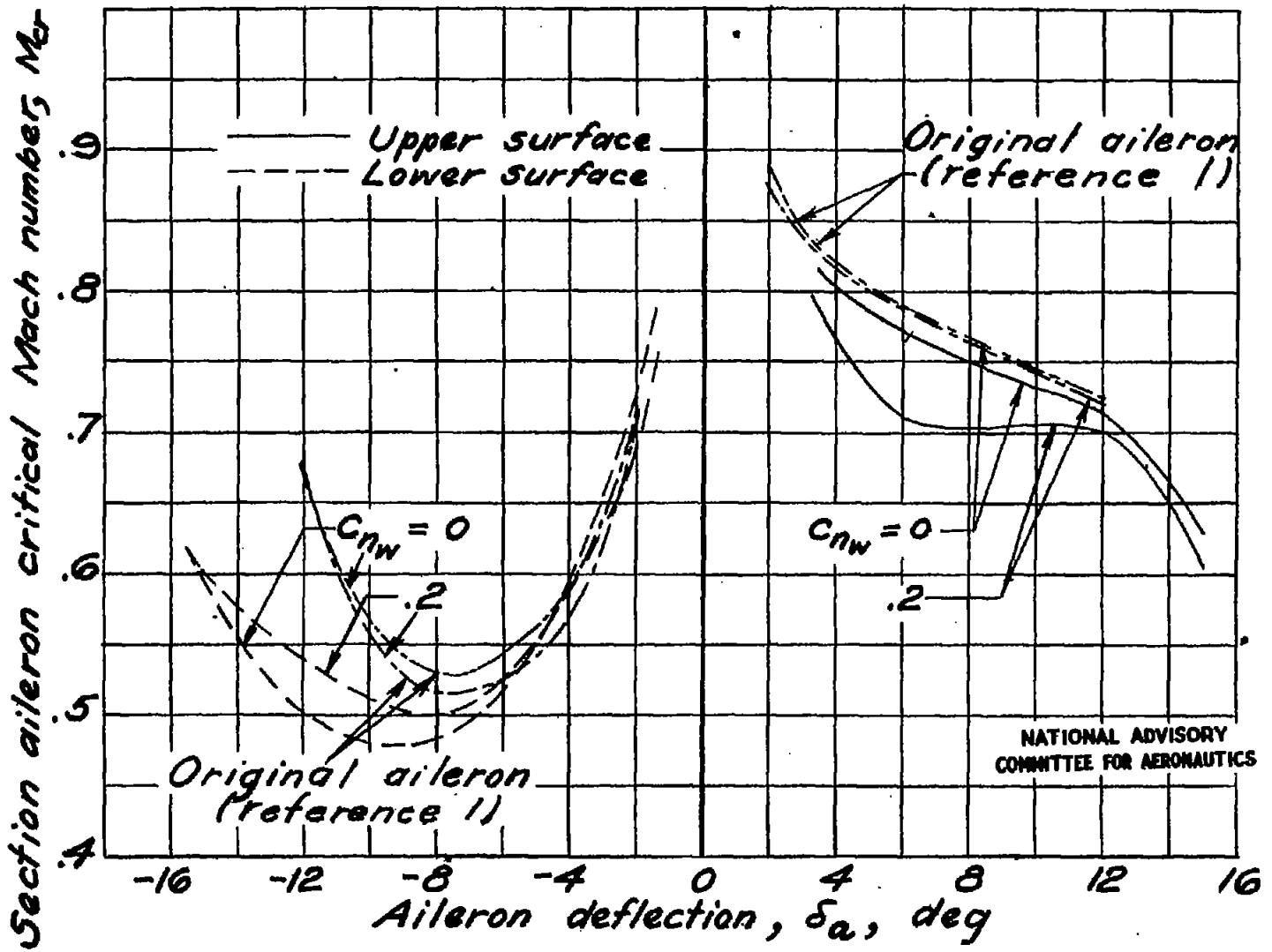

Figure 12.- Section critical Mach number of aileron against aileron deflection at two section airfoil normal-force coefficients.

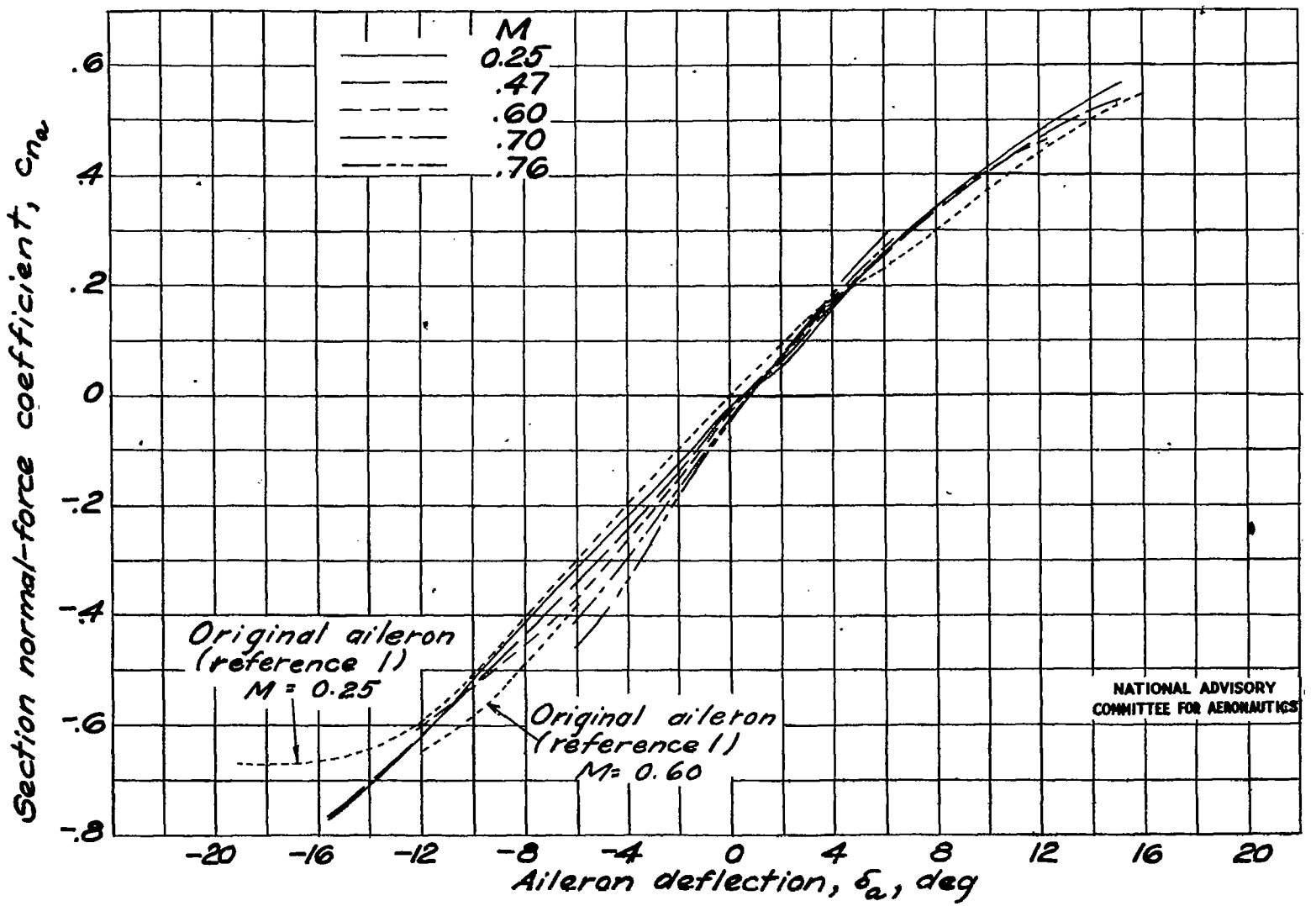

(a) $c_{n_w} = 0$.

Figure 13.- Section aileron normal-force coefficient against aileron deflection at various Mach numbers.

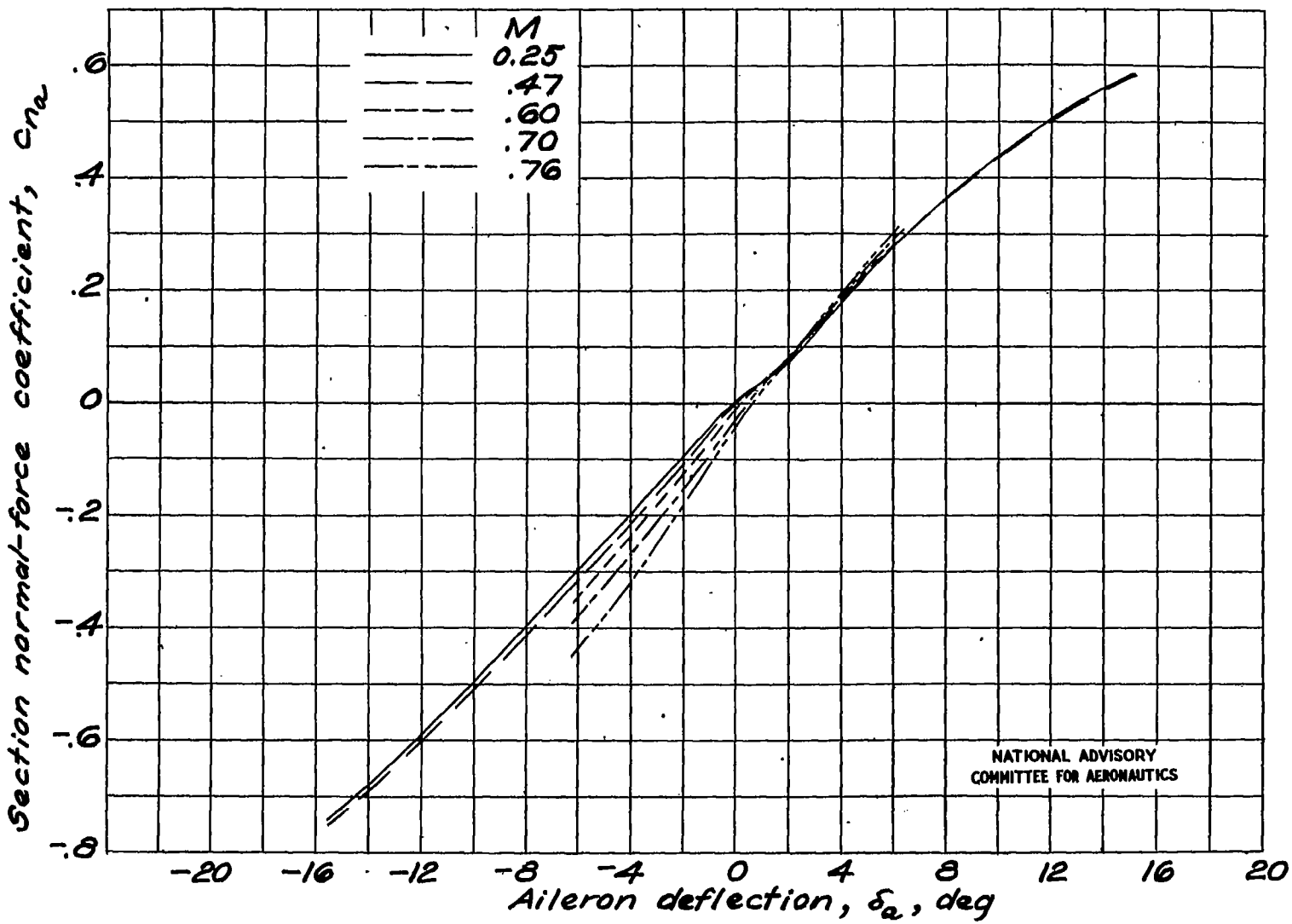

(b) $c_{n_w} = 0.1$.

Figure 13.- Continued.

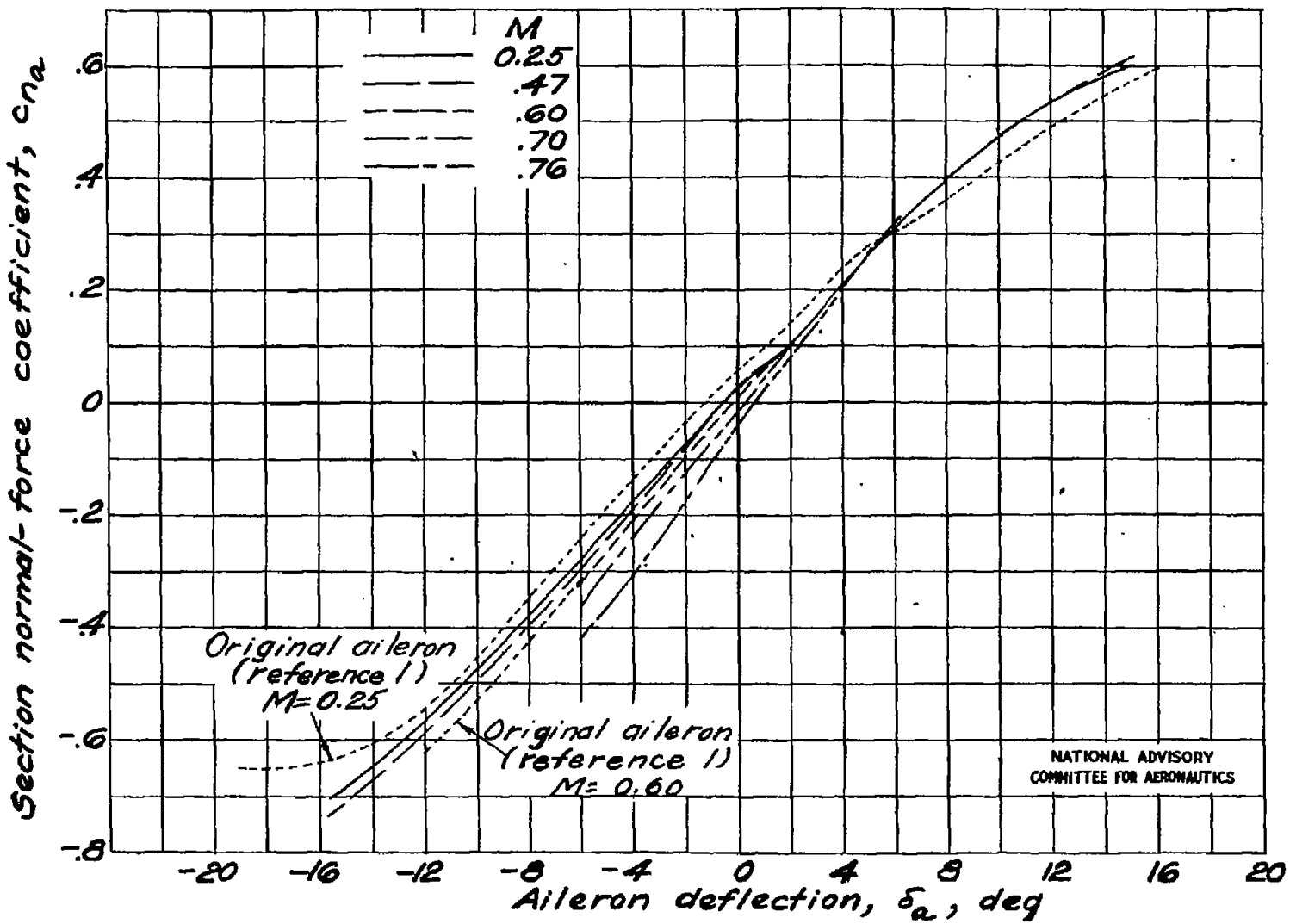

(c) c_{n_w} = 0.2.

Figure 13.- Concluded.

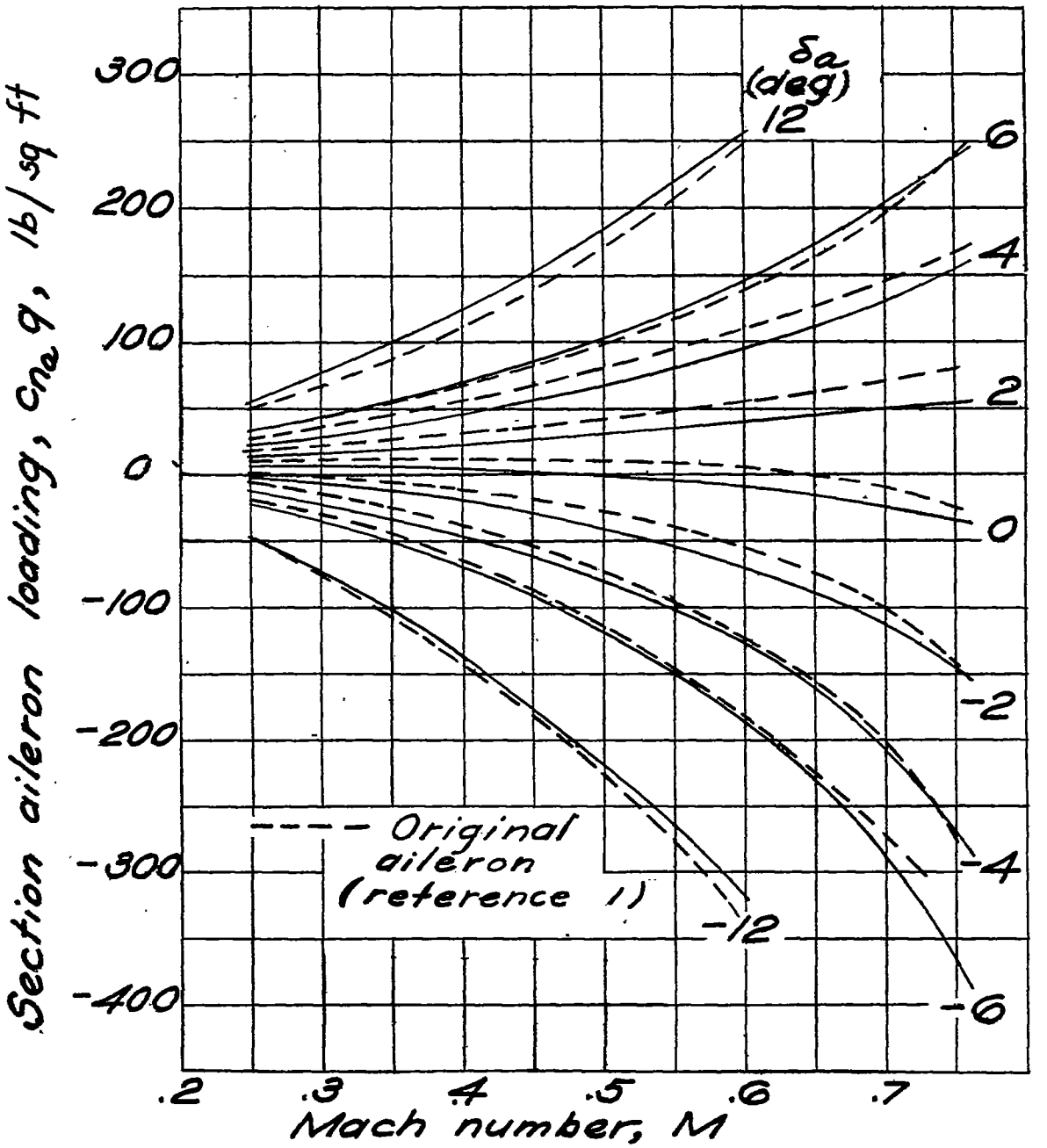

(a) Sea level.

Figure 14.- Section aileron loading at various aileron deflections for steady rate of roll.

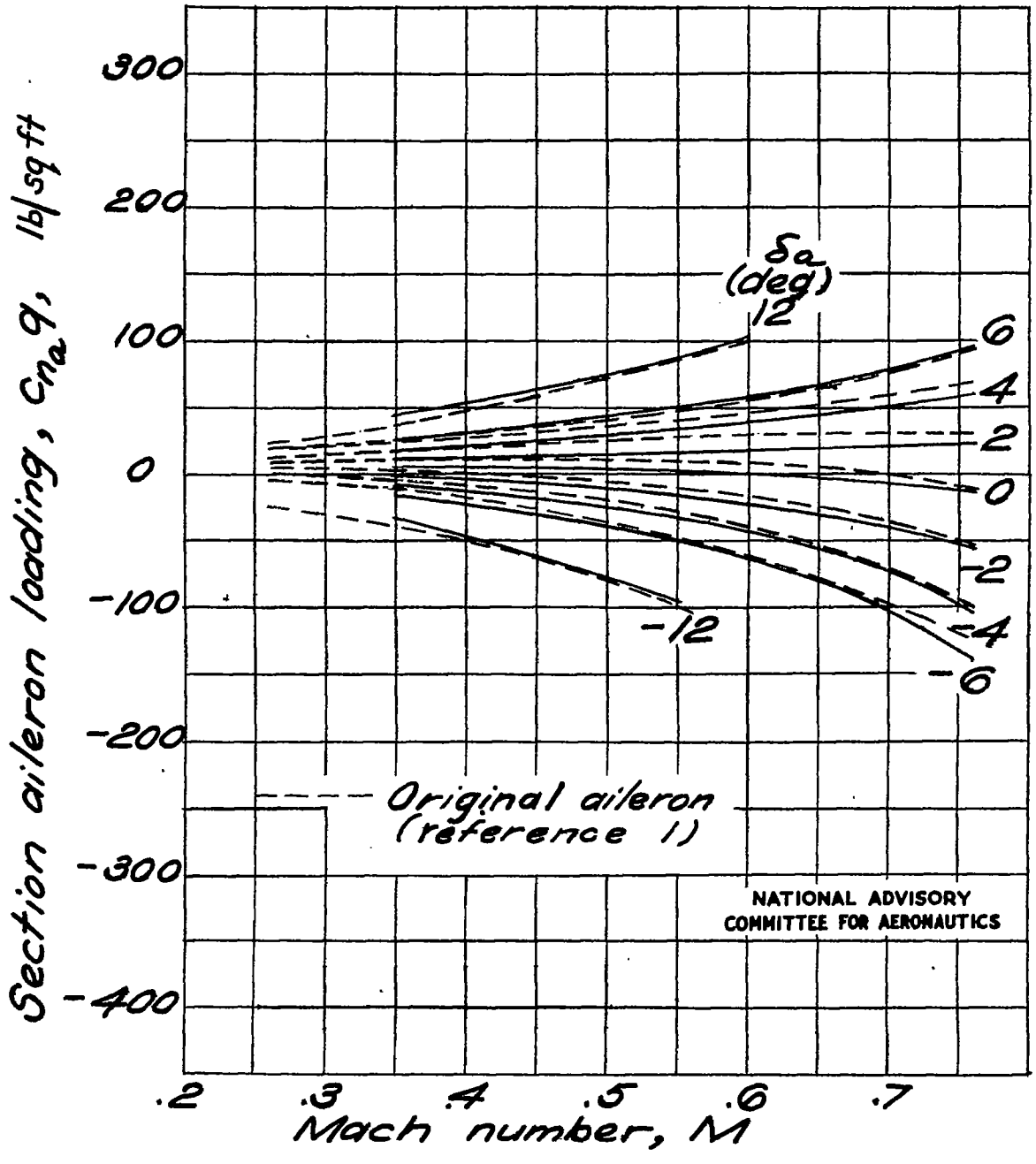

(b) 25,000 ft.

Figure 14.- Concluded.

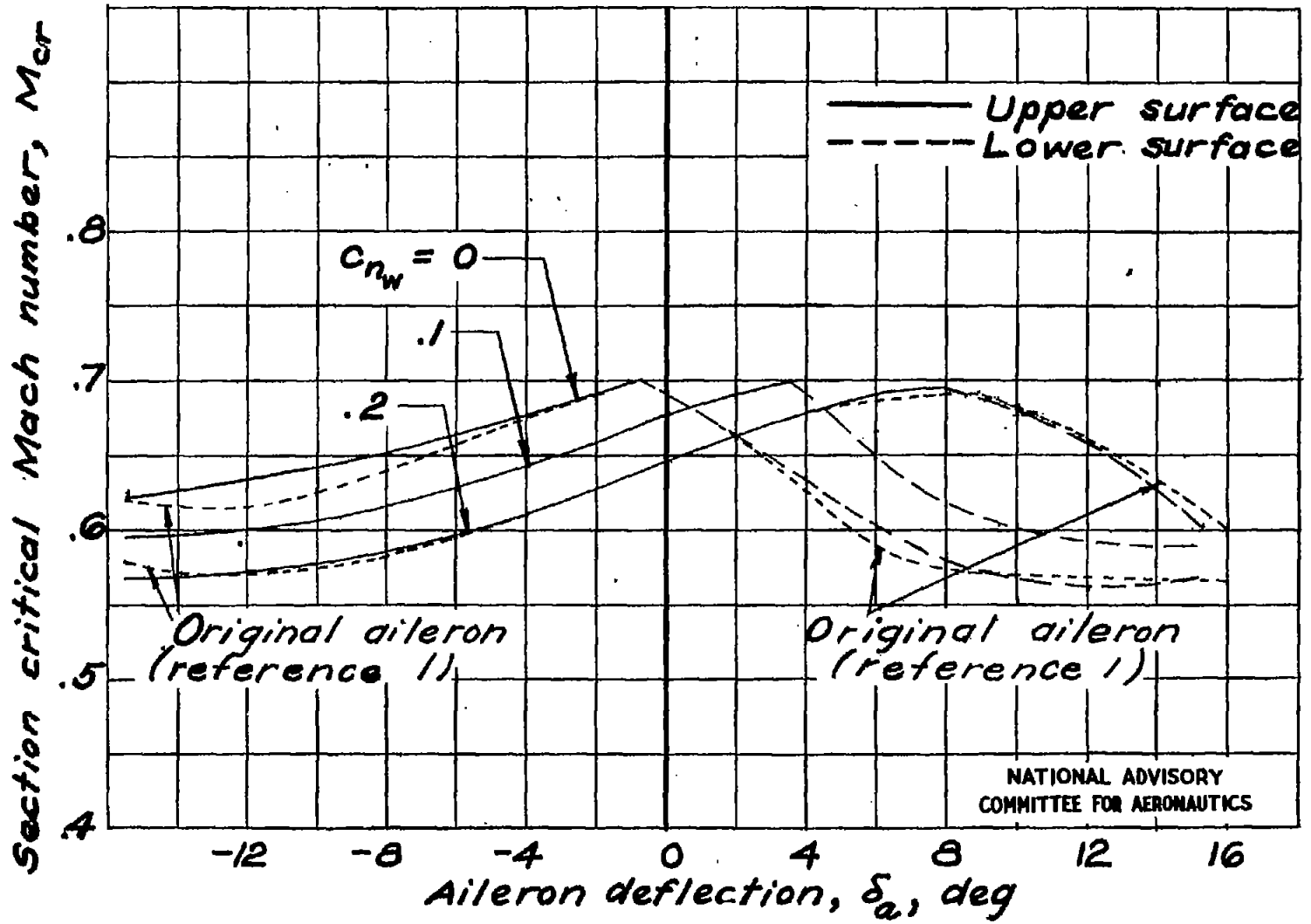

Figure 15.- Section critical Mach number of main portion of airfoil against aileron deflection at various section airfoil normal-force coefficients.

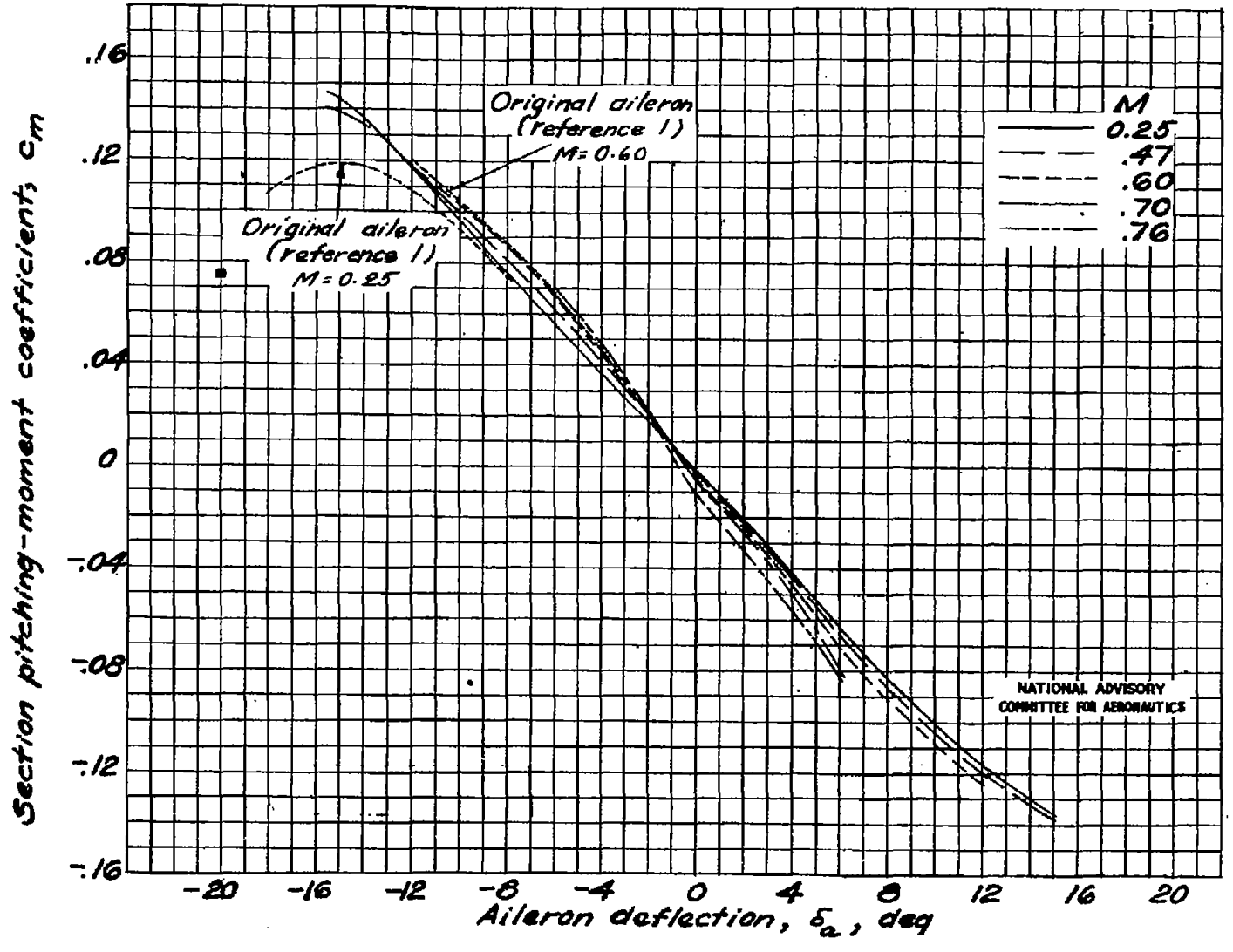

(a) $c_{n_w} = 0$.

Figure 16.- Section airfoil pitching-moment coefficient against aileron deflection at various Mach numbers.

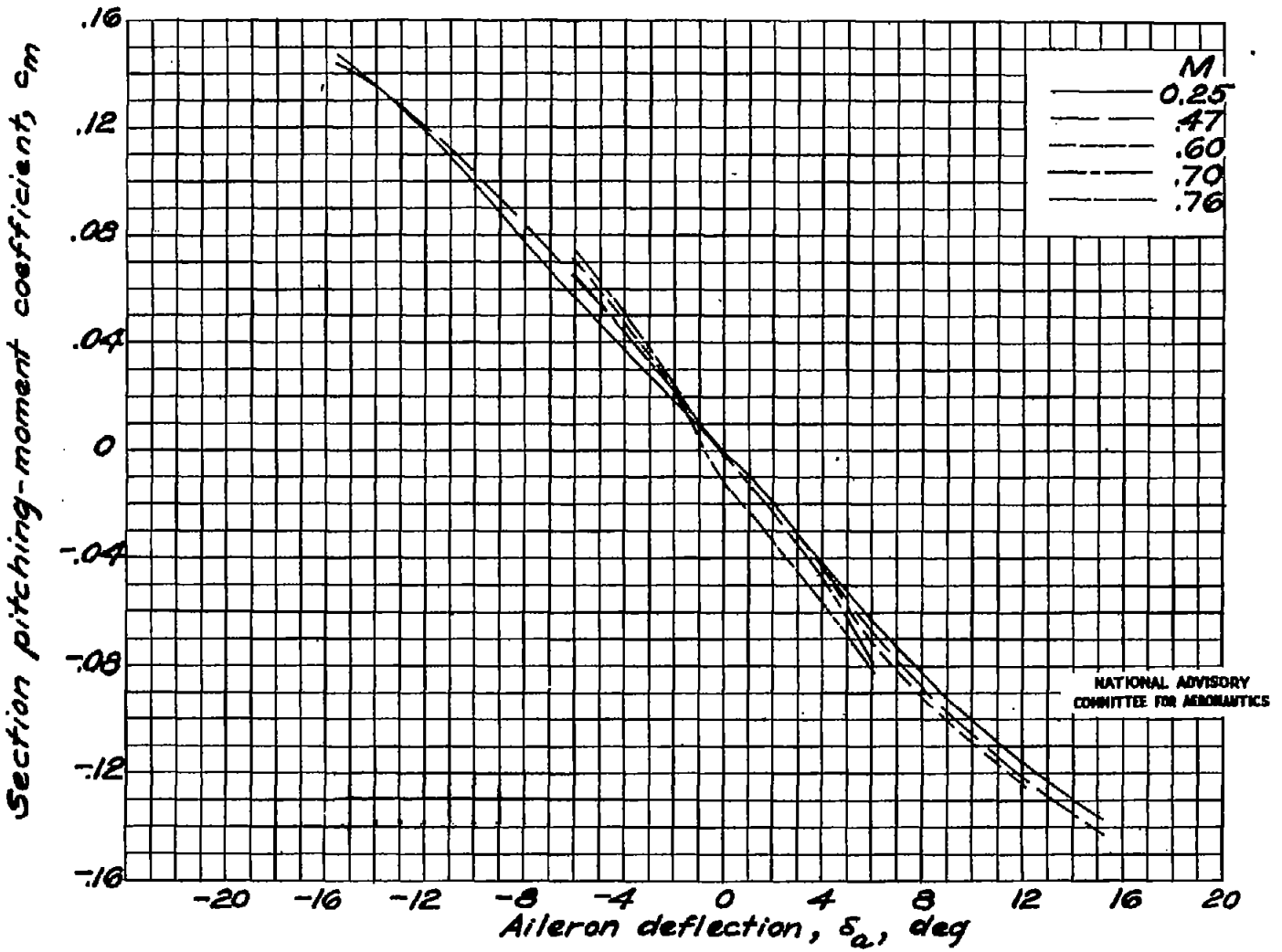

(b) $c_{n_w} = 0.1$.

Figure 16.- Continued.

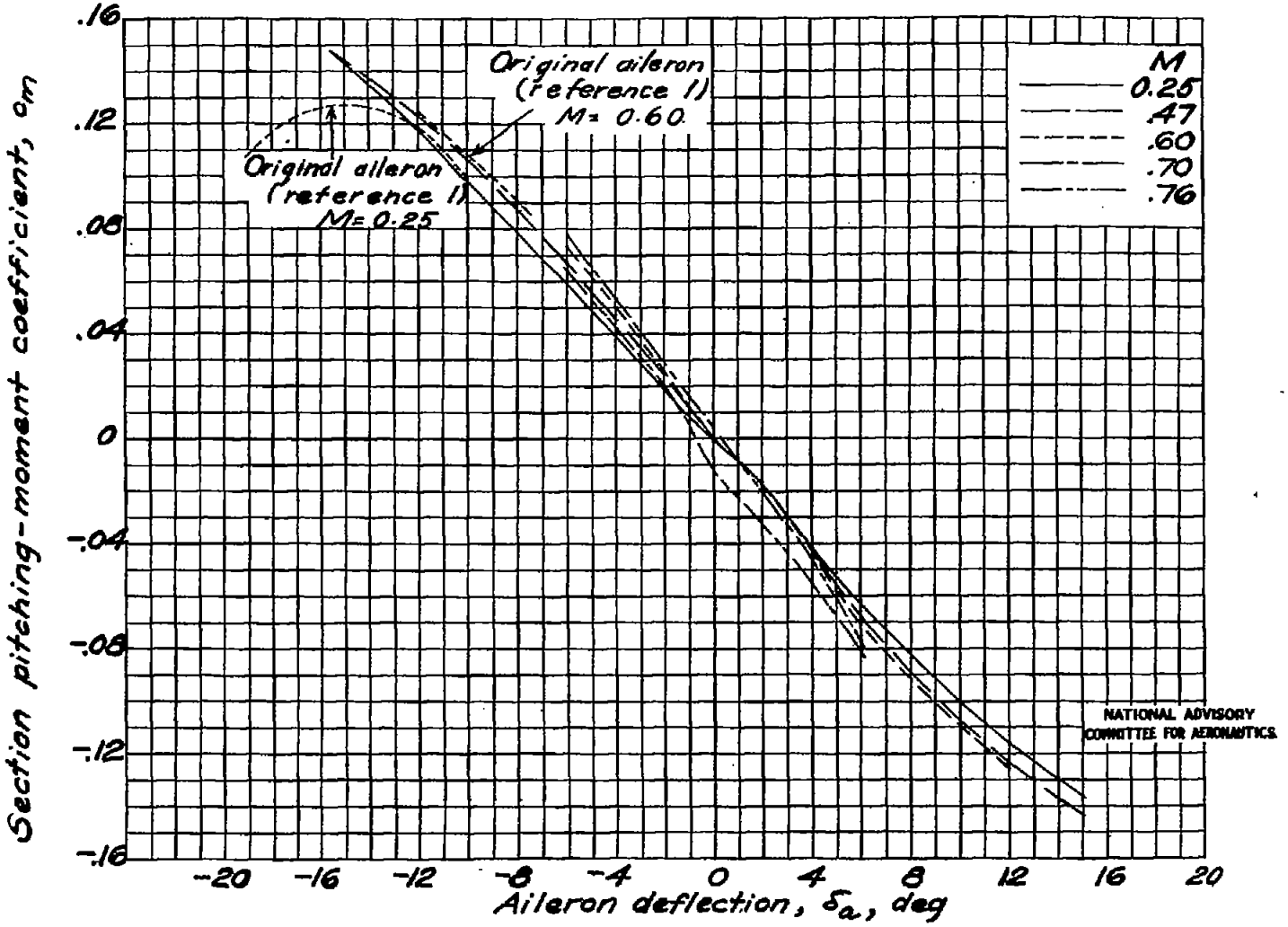

(c) c_{n_w} = 0.2.

Figure 16.- Concluded.

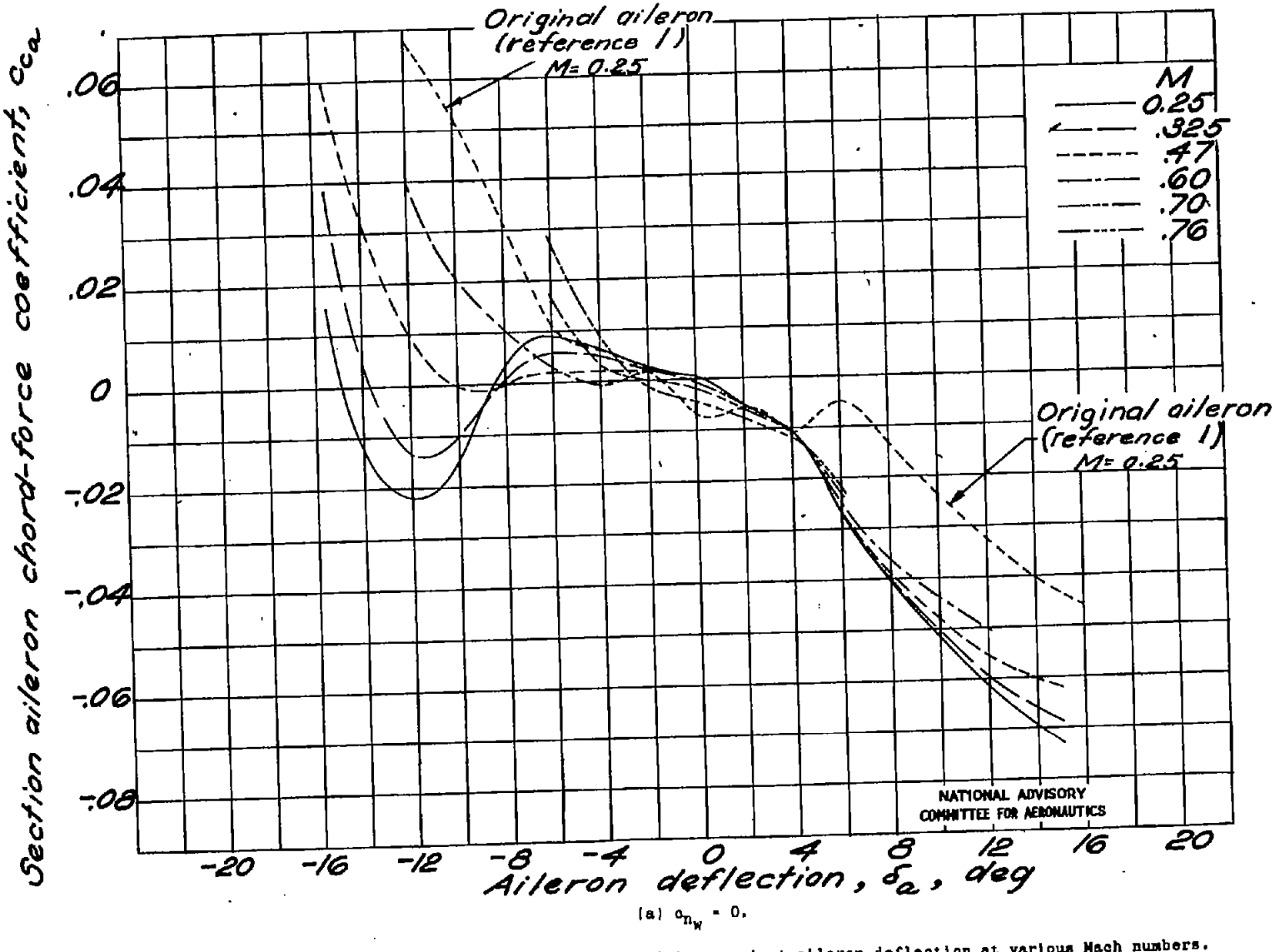

(a) $c_{n_w} = 0$.

Figure 17.- Section aileron chord-force coefficient against aileron deflection at various Mach numbers.

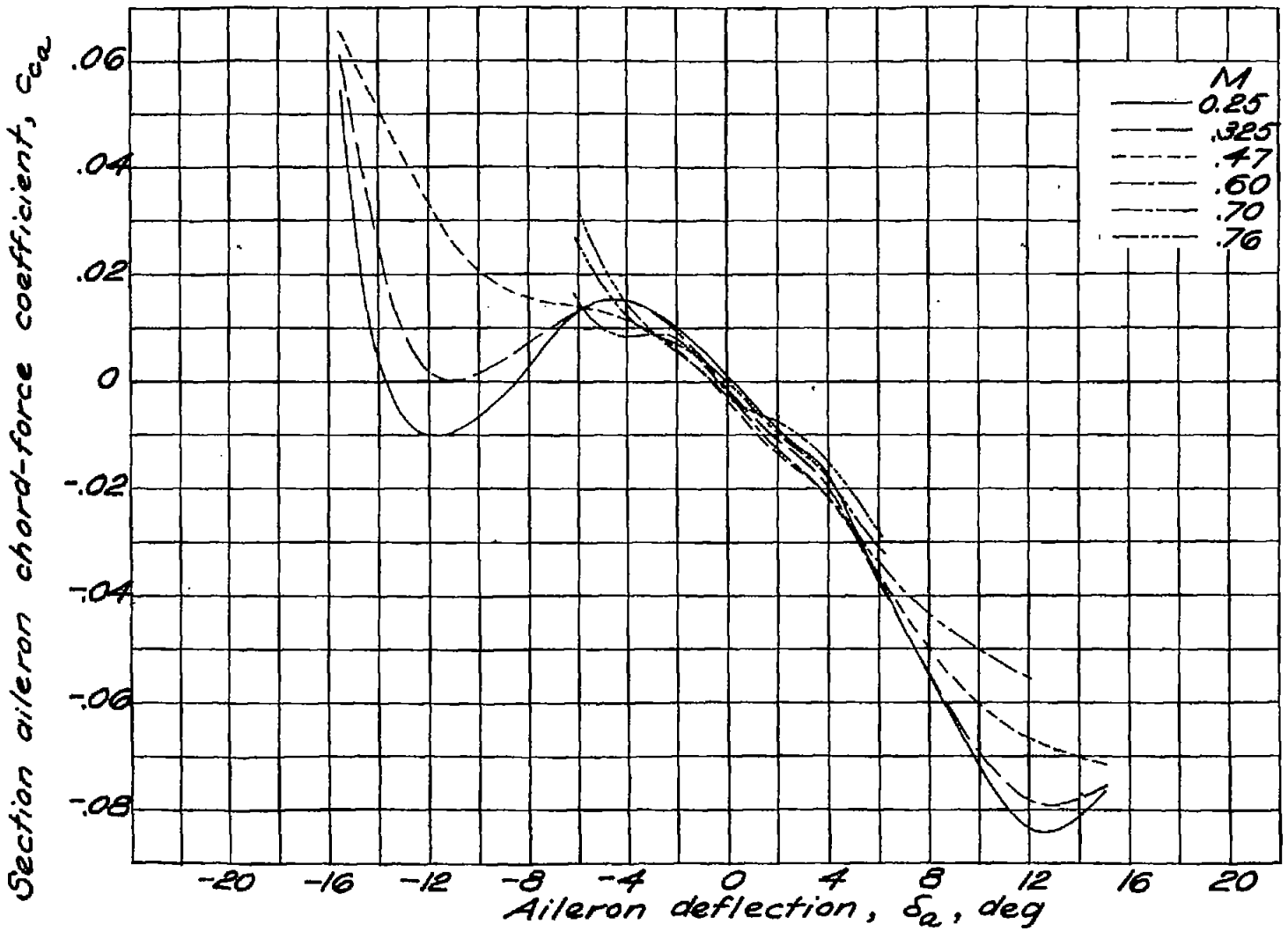

(b) $c_{n_w} = 0.2$.

NATIONAL ADVISORY COMMITTEE FOR AERONAUTICS

Figure 19.- Concluded.